Energy & Environmental Science

Accepted Manuscript

This article can be cited before page numbers have been issued, to do this please use: R. Koerver, W. Zhang, L. de Biasi, S. Schweidler, A. Kondrakov, S. Kolling, T. Brezesinski, P. Hartmann, W. Zeier and J. Janek, *Energy Environ. Sci.*, 2018, DOI: 10.1039/C8EE00907D.

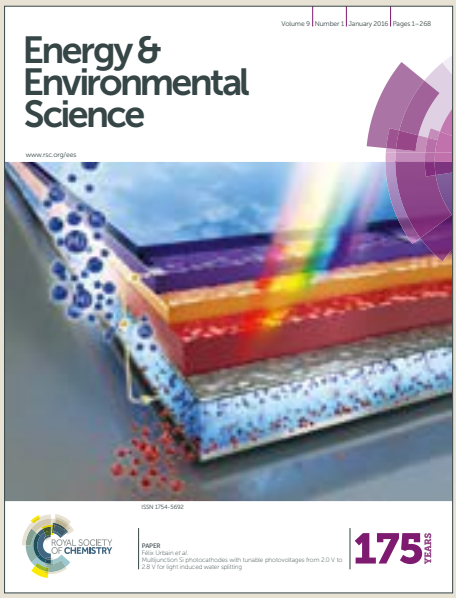

ROYAL SOCIETY OF CHEMISTRY

rsc.li/ees

View Article Online
DOI: 10.1039/C8EE00907D

Broader context

Lithium ion batteries are currently the most effective power storage technology for portable electronic devices and are envisioned to play a larger role in the next generation of electric vehicles. However, when considering the up-scale of current technologies, the employment of conventional organic liquid electrolytes presents a variety of safety issues, thereby motivating the search for safer and reliable battery architectures. Solid-state batteries that use a ceramic solid-electrolyte as a separator represent a promising alternative, which has received tremendous scientific and industrial interest in recent years. Notably, the intrinsic nature of a solid electrolyte brings in new considerations from a mechanical point of view. For example, most electrode materials undergo volumetric strain upon lithium insertion and extraction. The rigid environment is not necessarily able to compensate the mechanical changes induced by the electrodes, and thus, such changes must be carefully considered for this new technology. In this work, we present three unique approaches to probe the volumetric strain in electrode materials and highlight the importance of mechanical effects in solid-state systems. We hope to provide the reader with an overview of the relevant material properties and the potential issues that can occur when they are introduced to an operating system.

View Article Online
DOI: 10.1039/C8EE00907D

Chemo-mechanical expansion of lithium electrode materials – On the route to mechanically optimized all-solid-state batteries

Raimund Koerver[a,b], Wenbo Zhang[a,b], Lea de Biasi[c], Simon Schweidler[c], Aleksandr O. Kondrakov[d], Stefan Kolling[e], Torsten Brezesinski[c], Pascal Hartmann[d], Wolfgang G. Zeier*[a,b] and Jürgen Janek*[a,b,c]

[a]*Institute of Physical Chemistry, Justus-Liebig-University Giessen, Heinrich-Buff-Ring 17, 35392 Giessen, Germany.*

[b]*Center for Materials Research (LaMa), Justus-Liebig-University Giessen, Heinrich-Buff-Ring 16, 35392 Giessen, Germany*

[c]*Battery and Electrochemistry Laboratory (BELLA), Institute of Nanotechnology, Karlsruhe Institute of Technology, Hermann-von-Helmholtz Platz 1, 76344 Eggenstein-Leopoldshafen, Germany*

[d]*BASF SE, 67056 Ludwigshafen am Rhein, Germany*

[e]*Institute of Mechanics and Materials, Technische Hochschule Mittelhessen, Wiesenstraße 14, 35390 Giessen, Germany*

View Article Online
DOI: 10.1039/C8EE00907D

Abstract

Charge and discharge of lithium ion battery electrodes is accompanied by severe volume changes. In a confined space, the volume cannot expand, leading to significant pressures induced by local microstructural changes within the battery. While volume changes appear to be less critical in batteries with liquid electrolytes, they will be more critical in the case of lithium ion batteries with solid electrolytes and they will be even more critical and detrimental in the case of all-solid-state batteries with a lithium metal electrode.

In this work we first summarize, compare, and analyze the volume changes occurring in state of the art electrode materials, based on crystallographic studies. A quantitative analysis follows that is based on the evaluation of the partial molar volume of lithium as a function of the degree of lithiation for different electrode materials. Second, the reaction volumes of operating full cells ("charge/discharge volumes") are experimentally determined from pressure-dependent open-circuit voltage measurements. The resulting changes in the open-circuit voltage are in the order of 1 mV/100 MPa, are well measurable, and agree with changes observed in the crystallographic data. Third, the pressure changes within solid-state batteries are approximated under the assumption of incompressiblility, *i.e.* for constant volume of the cell casing, and are compared to experimental data obtained from model-type full cells. In addition to the understanding of the occurring volume changes of electrode materials and resulting pressure changes in solid-state batteries, we propose "mechanical" blending of electrode materials to achieve better cycling performance when aiming at "zero-strain" electrodes.

View Article Online
DOI: 10.1039/C8EE00907D

1. Introduction

The storage of alkali metals in anode (AAMs) and cathode active materials (CAMs) in alkaline ion batteries causes volume changes, with the magnitude depending on the mechanism of the storage processes.[1,2] In the case of lithium ion batteries (LIBs) with liquid electrolytes these volume effects have two major consequences: (a) The relatively large volume effects of high capacity AAMs cause damage to the solid electrolyte interphase (SEI) during charge/discharge cycling, as well as loss of active lithium, both of which lead to capacity fading.[3–5] (b) The anisotropic volume changes of primary CAM particles, despite being comparably small to the volume changes on the anode, lead to mechanical damage up to fracture in the secondary particle agglomerates of cathode materials at higher degrees of delithiation, which also causes capacity fading.[6–9] In batteries employing liquid electrolytes, all the resulting mechanical stress remains localized in the primary and secondary particles of the active materials because the electrode binder is plastic and the liquid electrolyte does not transfer stress. One may assume that this lack of stress transfer throughout the electrodes will also be the case for polymer batteries with sufficiently soft polymers.

In all-solid-state batteries (SSBs) with inorganic (ceramic) solid electrolytes (SEs) the situation changes dramatically.[10] Similar to the liquid electrolyte system, the SEI between the electrode materials and the SE will also be damaged by the volume changes of the electrodes and fracture of secondary particles will also occur in a SE environment. However, when an SE is employed the microstructure will experience mechanical stress and may itself suffer from the local volume changes.[8,11,12] This stress development needs to be considered when external pressure is applied, which was found to be particularly important for SSBs.[13] Obviously, the spatial distribution of the mechanical strain and stress will be complicated in a real battery, assuming a different distribution of the solid phases and complex porosity, depending on the processing technology. Electrode charge balancing has been known to play a crucial role in conventional LIBs.[14,15] In SSBs it needs to be considered whether mechanical balancing of the active materials and the SE, in terms of the compatibility, is also necessary. An unfavorable combination of electrode materials may be mechanically detrimental for the battery performance. On the other hand, it may very well be that it is possible to make use of the chemo-mechanics for the reduction of porosity in a mechanical formation step.[2,16]

View Article Online
DOI: 10.1039/C8EE00907D

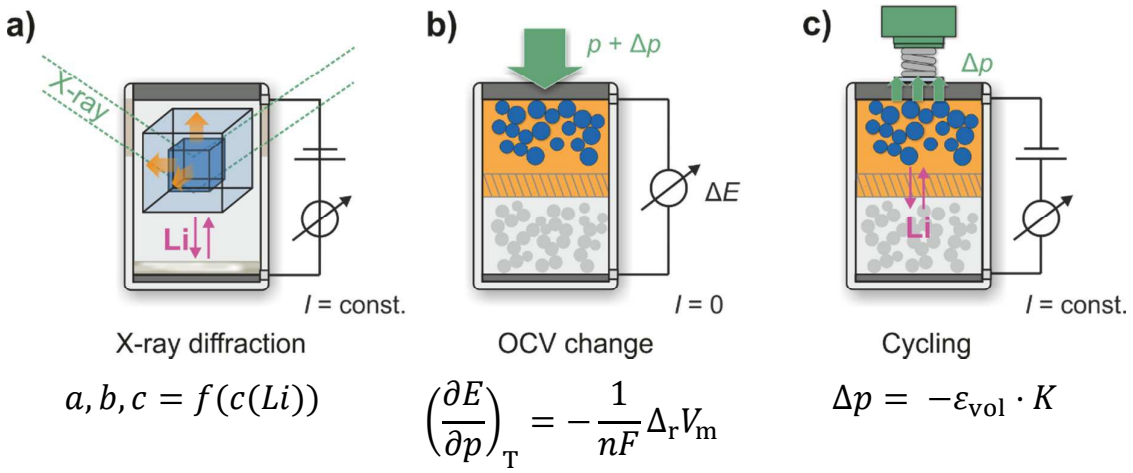

Figure 1: Schematic of the different experiments related to volume changes in electrode materials. (a) Measurement of the lattice parameters (a, b and c) of crystalline active materials by in or ex situ X-ray diffraction as function of SOC (state of charge), i.e. of lithium concentration. (b) Measurement of the OCV (E) as function of pressure p and evaluation of the reaction volume $\Delta_r V_m$ of the cell reaction, with n being the number of transferred electrons and F denoting the Faraday constant. (c) Monitoring the pressure change Δp of an operating cell, which in a first approximation can be described by the product of volumetric strain ε_{vol} and the bulk modulus K for small values of the strain.

Of course, mechanical issues of active and passive cell components, as well as the mechanical expansion of full cells, have already been addressed.[1,2,16–19] The issue of charge-dependent volume changes of electrode materials, the resulting pressure changes in volume-constrained solid-state batteries (as also in liquid electrolyte batteries), and the change of cell voltages upon external pressure have not been treated together systematically yet. The present work aims to fill this gap by discussing the formal background and presenting experimental data on pressure build-up and pressure-dependent voltage effects in solid-state batteries. The formal treatment is restricted to a relatively simple macroscopic picture, as any more detailed treatment will require numerical methods. In this work, we focus on a rather simple formal approach to obtain some general conclusions that may help design microstructurally improved SSBs.

The presented work is divided into three sections: In the first section, we review the volume changes of electrode materials, as obtained from *in situ* X-ray diffraction. The crystallographically monitored volumetric changes are then analyzed in terms of the partial molar volume of lithium (Figure 1a). The partial molar volume is a valuable concept in the

View Article Online
DOI: 10.1039/C8EE00907D

thermodynamics of solutions, and its value is very different for different modes of lithium storage, as shown in detail below, and it can be directly used to evaluate chemo-mechanical effects in full cells.

In the second section, we use these partial molar volumes to predict changes of cell voltages upon pressure increase. These voltage changes are typically small and on the order of a few mV, however, they can be used to evaluate the partial molar volume of lithium in electrode materials in an independent thermodynamic experiment. As the charge or discharge of a battery corresponds to the chemical cell reaction, the reaction volume $\Delta_r V_m$ of the cell reaction describes the pressure dependence of the open-circuit voltage (OCV). This reaction volume is the difference of the partial molar volumes of lithium in both electrodes, which indeed links the thermodynamic experiment with the diffraction data on the crystallographic volume expansion. To the best of our knowledge, this link is demonstrated here for the first time for batteries experimentally. In fact, we propose to use the terms *discharge volume* and *charge volume* in analogy to the term *reaction volume* in the case of chemical reactions.

If we use free mechanical boundary conditions of an operating battery, the battery can shrink or swell. In the final section, we measure the mechanical stress (which may be considered as pressure) induced in cells with constrained volume and compare the experimental results with theoretical estimations from the discharge volume and charge volume. For the sake of simplicity, we neglect the anisotropy of the materials and inhomogeneous stress fields and obtain a good agreement with experiments. The final discussion then includes the concept of two-phase mixture of electrode materials to minimize volume effects of electrodes by suitable material combinations and chemomechanical engineering.

Along with these three sections of the paper, we give an overview on the mechanical properties of SSB components and highlight their critical relevance when facing lithium induced stress. By carefully considering the volumetric effects of electrode materials and a reasonable choice of electrode materials and SEs, we want to enable the perspective to mechanically optimized all-solid-state batteries.

View Article Online
DOI: 10.1039/C8EE00907D

2. Chemical expansion of electrode materials

Active electrode materials are known to exhibit volume changes as a function of the lithium content[1,2,16] and the volume changes strongly depend on the storage mechanism.[1] While true solid solutions show mostly relatively small volume changes, two-phase systems or conversion-type systems may show much larger volume effects (with exceptions), similar to the lithium metal anode. These volume changes have been widely addressed in the literature but have rarely been summarized with a focus on net volume effects during cycling of LIBs. The reason is quite simple: Local volume changes of the active electrode materials are taken up by the liquid electrolyte and are transformed into (hydrostatic) pressure. The resulting swelling and shrinking of the jelly roll inside its container is well documented for typical LIBs.[20–24] We like to note that the anisotropic volume change of state-of-the-art cathode materials often leads to cracks in the secondary particles during cycling, which is one of the reasons for long-term cathode degradation.[7,25–29]

The mechanical boundary conditions of SSBs are quite different from LIBs and their liquid electrolytes. While the volume changes of the active materials are of course the same, independent of the type of electrolyte. However, the SE will not transform these volume changes simply into a macroscopic, homogeneous pressure, but will itself suffer from the resulting local stress due to elastic and plastic deformation. Cracks can occur between SE and active materials, or the SE may even locally be deformed such that its microstructure and local conductivity changes.[8,11,30–34] In summary, SSBs may experience severe mechanical degradation from the volume changes of the active electrode materials.

Typically, the volume change of a solid solution phase upon lithiation/delithiation is determined using X-ray diffraction.[25,35–38] Only in rare cases, data from dilatometric measurements are available in the literature.[39–41] The crystal structures of layered cathode materials like lithium cobalt oxide or chemically similar solid solutions such as $Li[Ni_{1-x-y}Co_xMn_y]O_2$, so-called "NCM" materials, exhibit reversible volume changes, in which the dependence on lithium content is not necessarily linear.[25,42–45] Additionally, the lattice parameter changes are usually not isotropic, and electrode materials expand/shrink differently along the various crystallographic axes. One would expect that CAMs undergo contraction of the lattice volume during delithiation (*i.e.* charging), and indeed most CAMs shrink during charging, as shown exemplarily in Figure 2a. $LiCoO_2$ is a rare exception, as Dahn and coworkers showed early on.[42] The unit cell volume of $LiCoO_2$ increases upon delithiation to $Li_{0.5}CoO_2$ by roughly +2 %.[42] When further lithium is extracted, the average charge at the

View Article Online
DOI: 10.1039/C8EE00907D

oxygen ions is assumed to decrease leading to smaller repulsion of oxygen layers that is reflected in a decrease of the Li-slab width and overall unit cell volume.[46,47] In contrast to LCO, the unit cell volume for NCM materials decreases (anisotropic) over the whole range of compositions. While the layered compounds exhibit unit cell expansions along the *z*-direction due to the higher Coulombic repulsion of the metal-oxygen layers, the *x*-*y*-directions directly depend on the nature and size of the transition metal. The magnitude of volume change of those materials thereby significantly depends on their stoichiometric composition.[25,35,37,48–50] In particular for nickel-rich compounds, the volume change is more severe, as they can be delithiated to a higher degree in a given potential range and nickel experiences the largest change in ionic radius upon transition metal oxidation.[25,35,37] For instance, $LiNi_{0.33}Co_{0.33}Mn_{0.33}O_2$ (NCM-111) will undergo a lower volume change during lithiation than $LiNi_{0.8}Co_{0.1}Mn_{0.1}O_2$ (NCM-811).[25,37,43–45] Similar observations were found for related systems like $LiNi_{0.8}Co_{0.15}Al_{0.05}O_2$ (NCA).[9]

AAMs also undergo reversible volume changes during lithiation/delithiation. In extreme cases such as silicon, the volumetric strain $\Delta V/V$ can be as high as 400 % during lithiation.[51] The volumetric strains of metal alloy electrodes such as indium are smaller, but even intercalation-type anode materials such as graphite exhibit significant expansion upon lithiation.[12,23,36] Graphite undergoes a volumetric strain of approximately 13 % upon full lithiation to Li_6C. Because of its multi-step lithiation process, the resulting volume change of the material is strongly non-linear (Figure 2b).[24,52–54]

The concept of chemical expansion can formally be transferred to two-phase systems, however, here the volume change upon lithiation is strictly linear, as only the phase fractions change as function of lithium content. Whereas the commonly employed lithium titanate $Li_4Ti_5O_{12}$ is known to be a so-called zero-strain material with a negligible volumetric strain of -0.2 % upon delithiation,[55,56] the widely used cathode material lithium iron phosphate $LiFePO_4$ exhibits a two-phase transition with a volume strain of approximately -7 % from $LiFePO_4$ to $FePO_4$.[2,38,57]

Chiang and co-workers addressed volume change of lithium intercalation compounds for usage as micro-electromechanical actuators and provided a selection of electrode materials and their volume change.[2,16] It is instructive to consider the different volume strains from a more general point of view, as it is provided by thermodynamic relations, e.g. for solutions. All volume effects of solutions can be broken down to the partial molar volume of lithium in the respective compounds. Intercalation or insertion of lithium necessarily leads to a volume

View Article Online
DOI: 10.1039/C8EE00907D

change that is formally described by the partial molar volume $\bar{V}_{\mathrm{m}}(\mathrm{Li})$ of lithium. The partial molar volume is defined as the differential of the volume of the homogeneous phase under consideration, caused by adding lithium (and keeping all other state variables constant, *i.e.* pressure p, temperature T and amount of phase in the system n_{i}),

$$\bar{V}_{\mathrm{m}}(\mathrm{Li}) \equiv \left(\frac{\partial V}{\partial n(\mathrm{Li})}\right)_{T,p,n_{\mathrm{i}}\neq n_{\mathrm{Li}}} . \quad (1)$$

The partial molar volume of lithium is positive if the volume of a solution increases upon adding lithium. It is itself a function of the lithium content, as the insertion/extraction mechanism may change with lithium content and it provides direct information on chemical expansion. In contrast to relative volume changes, *i.e.* the volumetric strain, it represents the absolute volume change upon lithiation (by integration):

$$\Delta V = \int_{n(\mathrm{Li})_1}^{n(\mathrm{Li})_2} \bar{V}_{\mathrm{m}}(\mathrm{Li}) dn(\mathrm{Li}). \quad (2)$$

Figure 2a summarizes the crystallographic data obtained for a number of commonly employed cathode materials.[35,37] By correlating the change in the unit cell volume to the change in lithium content gives the partial molar volume in the respective compound. Using the high resolution of the available crystallographic data allows to derive the partial molar volume of lithium. Lithium metal can be considered as a reasonable natural reference for the partial molar volume values. Its molar volume of $V_{\mathrm{m}}(\mathrm{Li})$ = 12.97 cm³/mol at 298 K can also be understood as the volume of a lithium atom in the Li metal lattice on the microscopic scale, and it may be considered as a kind of typical upper limit of the volume change that a solution may experience upon addition of Li. However, the partial molar volume of Li in any other solution-type phase depends on the mechanism of the Li uptake on atomic scale, and the data in Figure 2b shows that the partial molar volume of lithium in high-Ni NCM and in NCA at very low Li content is larger than the molar volume of Li metal. This clearly indicates that severe changes in chemical bonding occur when these Ni-rich cathode materials are strongly delithiated.

In the case of two-phase systems like $Li_4Ti_5O_{12}$/$Li_7Ti_5O_{12}$ (LTO) or $FePO_4$/$LiFePO_4$ (LFP), the concept of the partial molar volume as a solution property becomes formally incorrect, as the storage process is accompanied by a phase transformation. The volume change is then formally better considered as molar reaction volume (of phase formation) $\Delta_{\mathrm{r}}V_{\mathrm{m}}(\mathrm{Li})$. It is constant and thus independent of the Li content of the two-phase active material, provided that no internal stress is built up during lithiation or delithiation. Thus, when indium

View Article Online
DOI: 10.1039/C8EE00907D

(V_m(In) = 15.71 cm³/mol) is lithiated, the formation of the intermetallic phase InLi (V_m(InLi) = 23.60 cm³/mol) leads to the reaction volume of $\Delta_r V_m(\mathrm{In/InLi}) = +7.89$ cm³/mol.[11] For the sake of a simple representation of the data, we will consider this reaction volume of two-phase active materials as an apparent partial molar volume of lithium $\bar{V}'_m(\mathrm{Li})$.[11] In general, the reaction volume $\Delta_r V_m$ of adding Li to a given compound (e.g. $Li_4Ti_5O_{12}$) and forming a different (lithiated) compound corresponds formally to the partial molar volume $\bar{V}_m(\mathrm{Li})$ of Li in a solution-type electrode. The full notation of the partial molar volume then reads as $\bar{V}_m(\mathrm{Li, phase\ \alpha})$, describing the differential volume effect of phase α in m³/mol, when a small amount of Li is added. Here, we will denote the apparent partial molar volume of two-phase active materials as $\bar{V}'_m(\mathrm{Li, delithiated\ phase\ \alpha/lithiated\ phase\ \beta})$.

For $LiFePO_4$ (LFP), the volume effect of lithiation is also linear and is caused by the formation of the crystalline LFP by lithiation of the $FePO_4$ (FP) phase, which results in an apparent partial molar volume $\bar{V}'_m(\mathrm{Li, FP/LFP}) = +11.62$ cm³/mol.[38] For the zero-strain material LTO the change in volume is negligible, resulting in a partial molar volume of Li of virtually zero.[55,56] Silicon is known to experience extreme volume changes, however, its fully lithiated phase is amorphous. In order to enable a comparison towards other electrode materials, we focus on the reaction volume between the two crystalline phases α-Si (cubic) and $Li_{15}Si_4$ (metastable crystalline).[58,59] The partial molar volume derived for one equivalent lithium is then 8.85 cm³/mol and thus in the range of indium metal. However, its capability of lithium uptake (3580 mAh/g) of more than 3.75 lithium atoms per Si atom creates a high volumetric change.[58,59] Please note that Figure 2 is restricted to the uptake of 1 mole of Li per formula unit, in order to allow for better comparison of the different materials. While silicon is usually considered as a material with a particularly large volume effect, the partial molar volume of Li in silicon is not much different from the partial molar volume of Li in indium. Another particular case is graphite. The partial molar volume of lithium as a function of the lithium content is highly non-linear: Because of the staging behavior during lithium intercalation $\bar{V}_m(\mathrm{Li, graphite})$ shows a strong dependence on the state of lithiation. The volume effects during lithiation of graphite, as determined by using *operando* XRD, have only recently been reported quantitatively.[36]

View Article Online
DOI: 10.1039/C8EE00907D

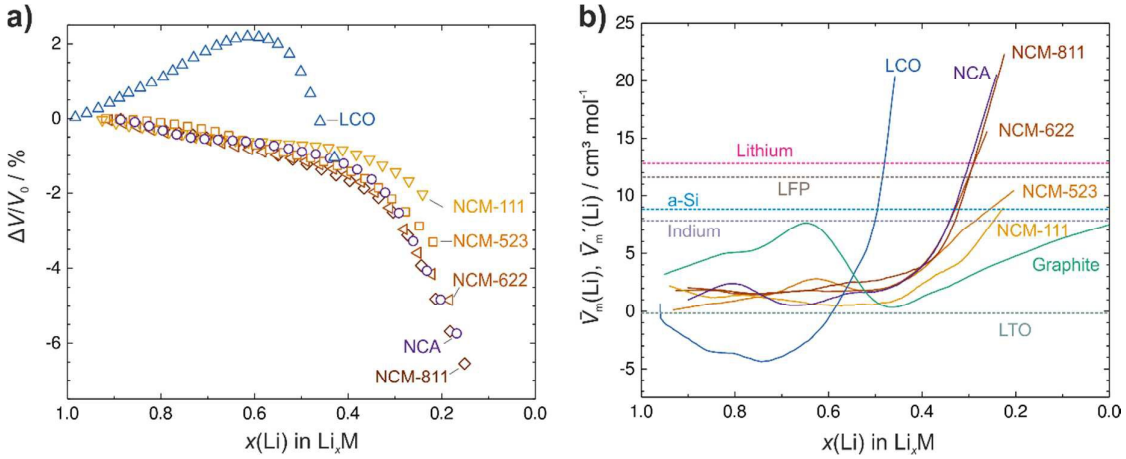

Figure 2: a) The unit cell volume obtained from crystallographic data versus the state of lithiation of positive electrode materials.[35,37] *b) Survey of available data for the partial molar volume* $\bar{V}_m(Li)$ *of Li in homogeneous storage phases or the apparent partial molar volume* $\bar{V}_m'(Li)$ *in two-phase electrode materials. All data for NCM materials, LCO and graphite were obtained from crystallographic data [LCO in this work, others see references*[35–37]*]. Additional data were extracted from the respective literature cited in the text. Please note that the x-axis shows in the direction of decreasing lithium content in a material* Li_xM*, i.e. in the direction of delithiation.*

Except lithium cobalt oxide (LCO), all active materials regarded in here exhibit a positive partial molar volume of lithium (Figure 2b). When lithium atoms are removed from LCO, the Coulomb repulsion between the MO_2 layers increases and thus the partial molar volume of lithium changes sign to positive values for $x < 0.6$, *i.e.* close to half-delithiation. In case of the NCM materials, this effect of Coulombic repulsion is overcompensated anisotropically by the strong size reduction of the Ni ions from Ni^{2+} to Ni^{4+}.[37] This compensation leads to a small positive partial molar volume, which increases steeply for $x < 0.4$ when a and c axis shrink simultaneously.

In general, when lithium is inserted into an electrode active material (except LCO), its volume increases, even though the relationship is not necessarily linear. In a first instance, this is beneficial for battery systems, as cathode and anode active material will exhibit volume changes in the opposite direction and thus reduce the net pressure of the battery system during cycling. However, certain combinations of electrodes that expand simultaneously, e.g. LCO combined graphite or lithium, can lead to strong net volume effects. LTO/NCM cells on the other hand will exhibit only very small net volume changes. In general, the locally generated

View Article Online
DOI: 10.1039/C8EE00907D

stress and its effects on the battery performance should be considered and evaluated for each material combination independently. Depending on the stiffness of the battery system, the employment of zero-strain anodes and cathodes or pressure mitigating electrode combinations - as presented later in this work - may be beneficial.[60–62]

3. The reaction volume of operating cells (E_{oc} = f(p))

Apart from the partial molar volume or reaction volumes obtained from crystallographic measurements, the volume change of electrode materials can be derived thermodynamically from operating solid-state battery cells. In the following, we present this second approach to evaluate the partial molar volume of lithium in electrode materials from the reaction volume $\Delta_r V_m$ of full cells using the open circuit potential (OCV), E_{oc}. Thermodynamic considerations state that the pressure dependence of the OCV of a battery is governed by the reaction volume:[63]

$$\left(\frac{\partial E_{oc}}{\partial p}\right)_{T,n_i} = -\frac{1}{nF}\Delta_r V_m. \quad (3)$$

A cell reaction with a positive reaction volume will show a decreasing OCV with increasing pressure, *i.e.* the thermodynamic driving force of the cell reaction with positive reaction volume is reduced with increasing pressure. The OCV is considered positive for the operation mode of a galvanic cell, *i.e.* the negative free enthalpy of the cell reaction ($\Delta_r G < 0$) drives the discharge of the cell. Thus, for a given cell reaction with Li_mAn and Li_rCat being the anode and cathode materials, before the discharge step and with x being the amount of exchanged Li upon discharge:

$$Li_mAn + Li_rCat \longrightarrow Li_{m-x}An + Li_{r+x}Cat \quad , \quad (4)$$

the reaction volume results as:

$$\Delta_r V_m(\text{discharge}) = \frac{\Delta_r V}{x} = \bar{V}_m(Li_rCat) - \bar{V}_m(Li_mAn). \quad (5)$$

If the partial molar volumes of lithium in the anode and the cathode compensate each other, the reaction volume is zero and the OCV will show no pressure dependence at all. In this study, the change of the OCV of the solid-state battery cells InLi | LGPS | LTO/LGPS and InLi | LGPS | LCO/LGPS was monitored while the applied pressure was incrementally ramped up (Supplementary Figure 1a and b). InLi is used to avoid side reactions as in the case of lithium metal.[64] Upon pressure increase, the OCV increases linearly as implied by

View Article Online
DOI: 10.1039/C8EE00907D

Equation (3). We assume that $\bar{V}_{\mathrm{m}}(\mathrm{Li,LTO})$ is the same for $Li_4Ti_5O_{12}$ and $Li_7Ti_5O_{12}$ due to the minor volume change.[55,56] Then only the indium anode contributes to the reaction volume in the In/LTO cell in Equation (6):

$$\Delta_{\mathrm{r}}V_{\mathrm{m}}(\mathrm{discharge,In/LTO,}) \cong -\bar{V}_{\mathrm{m}}(\mathrm{Li_mAn}) = -\bar{V}'_{\mathrm{m}}(\mathrm{Li,In/InLi}). \quad (6)$$

From linear regression of the experimental data, we obtain $(\partial E_{oc}/\partial p)_T$ = +0.122 mV/MPa, which leads to

$$\bar{V}'_{\mathrm{m}}(\mathrm{Li,In/InLi}) \cong -\Delta_r V_{\mathrm{m}}(\mathrm{discharge,In/LTO}) = F\left(\frac{\partial E_{oc}}{\partial p}\right)_{\mathrm{T}} \cong +11.81\,\frac{\mathrm{cm}^3}{\mathrm{mol}} \quad (7)$$

which is higher than the value of +7.89 cm³/mol for the crystallographic reaction volume of the phase transition between In and InLi by about +50% (compare to Figure 2b).[11] Thus, the OCV appears to be more affected by the applied pressure than predicted by the volume data obtained from the crystallographic data. In the case of the In/LCO cell, $\bar{V}_{\mathrm{m}}(\mathrm{Li,LCO})$ depends on the lithiation state of LCO while the InLi volume is independent of the molar fraction of Li. Hence, the OCV was measured at different SOCs. Again, for each *x*(Li) in LCO the OCV of the cell shows a linear dependence on *p* which yields $\Delta_{\mathrm{r}}V_{\mathrm{m}}$. The pressure dependence of the OCV is shown in Figure S1 in the Supporting Information. The reaction volume of the In/LCO is related to the pressure dependence of the OCV according to

$$\Delta_r V_{\mathrm{m}}(\mathrm{discharge,In/LCO}) = \bar{V}_{\mathrm{m}}(\mathrm{Li,LCO}) - \bar{V}'_{\mathrm{m}}(\mathrm{Li,In/InLi}) = -F\left(\frac{\partial E_{\mathrm{oc}}}{\partial p}\right)_T. \quad (8)$$

And thus,

$$\bar{V}_{\mathrm{m}}(\mathrm{Li,LCO}) = \bar{V}'_{\mathrm{m}}(\mathrm{Li,In/InLi}) - F\left(\frac{\partial E_{\mathrm{oc}}}{\partial p}\right)_T. \quad (9)$$

We can either use the experimental value $\bar{V}'_{\mathrm{m,exp}}(\mathrm{Li,In/InLi})$ = 11.81 cm³/mol or the crystallographic (theoretical) reaction volume $\bar{V}'_{\mathrm{m,XRD}}(\mathrm{Li,In/InLi})$ = 7.89 cm³. In Figure 3 we used the latter value to evaluate the partial molar volume $\bar{V}_{\mathrm{m,exp}}(\mathrm{Li,LCO})$ of Li in LCO depending on the SOC. A table of the exact slopes obtained by linear regression and data for $\bar{V}_{\mathrm{m}}(\mathrm{Li,LCO})$ using $\bar{V}'_{\mathrm{m}}(\mathrm{Li,In/InLi})$ from the OCV experiment can be found in the Supporting Information. Exemplarily we calculate the partial molar volume of Li in $Li_{0.8}CoO_2$ from the measured pressure effect $(\partial E_{\mathrm{oc}}/\partial p)_T = 0.102$ mV/MPa:

$$\bar{V}_{\mathrm{m}}(\mathrm{Li,Li_{0.80}CoO_2}) = 7.89\,\frac{\mathrm{cm}^3}{\mathrm{mol}} - 9.84\,\frac{\mathrm{cm}^3}{\mathrm{mol}} = -1.95\,\frac{\mathrm{cm}^3}{\mathrm{mol}}. \quad (10)$$

View Article Online
DOI: 10.1039/C8EE00907D

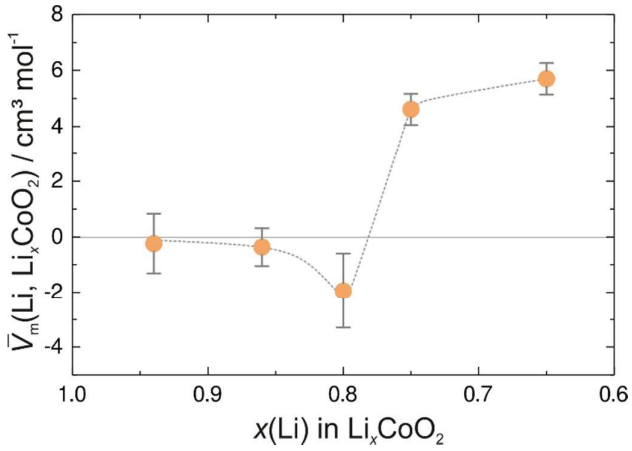

Figure 3: *Partial molar volume of Li in Li_xCoO_2 as function of x, evaluated from pressure dependent OCV measurements of In/LCO cells. In agreement with crystallographic data the partial molar volume of lithium in LCO is negative in the lithiated state and then turns positive upon delithiation. While the general trend agrees with the crystallographic data, diffraction data suggests the sign reversal at a lower lithium content of x(Li) = 0.6.*

The partial molar volume of Li in LCO as determined from the OCV pressure dependence ranges from −2 to +6 cm³/mol. Whereas the data agree qualitatively with the crystallographic data, the sign reversal occurs at higher lithium content than observed in the diffraction data. We believe that this difference is mainly due to the non-ideal pressure experiment. In fact, pressure is not applied uniformly but uniaxially, and orientation of the anisotropic CAM particles may not be perfectly random. Other sources of error may also add to the measurement uncertainty. For instance, irreversible lithium uptake in the cathode through LGPS oxidation may change the lithiation state of the active material.[65,66] Furthermore, only if the applied pressure is transferred completely to the LCO, the OCV will reflect the full pressure. Thus, non-isochoric plastic deformation as well as the porosity of the SE may influence the OCV measurement under pressure.

Nevertheless, despite the small pressure effects, the results for the partial molar volume of lithium are not only in the same order of magnitude but are even relatively close to the lithium molar volumes obtained from the crystallographic data. These results further allow to estimate the differences in local chemical potential of lithium in differently strained region of a CAM particle. In other words, the OCV of the solid-state battery itself will depend on the external and internal pressure and it is important to realize that the external battery setup will influence the cell voltage.

View Article Online
DOI: 10.1039/C8EE00907D

4. Pressure build-up in operating cells

While even severe pressure changes on the order of 1 MPa cause only relatively small OCV changes of around 0.1 mV, as demonstrated in Section 3, the volume changes of electrode materials will lead to substantial pressure effects (stress) in volume-constrained cells. Unfavorable combinations of active electrode materials can result in significant local stress inside the cell and may cause large overall pressure. If both, the cathode and the anode material, are expanding during the charging process (e.g. in a cell using LCO as cathode and lithium metal or graphite as anode), the system will experience the resultant stress of both chemical expansions. On the other hand, contraction during discharge will result in an overall reduced stress. Depending on the type of electrodes and the mechanics of the separator, a solid-state battery will experience *chemo-mechanical crosstalk* of the electrodes.

Consequences of the volume effects and stress induced in batteries have been considered from different perspectives, both for conventional LIBs as well as more recently for SSBs.[6–8] The stress generation model by Christensen and Newman, who predict fracture in active electrode materials, is widely used. Critical parameters in that model are lattice constants and particle sizes.[67,68] During delithiation, the overall lattice volume expansion (LCO) or contraction (NCM) can lead to so-called *lithium induced stress,* which is known to cause secondary particle fracture and eventually pulverization.[7] The stress developed during the lithiation/delithiation reaction can influence the reaction itself, e.g., compressive stress can decrease the lithium solubility in the electrode material, as shown by Chiang and coworkers in the case of $LiFePO_4$.[69]

One may expect that solid-state batteries will be severely affected by mechanical stress and strain. The chemically induced local stress couples with the external pressure, which is applied in order to increase the contact areas of electrodes and reduce charge transfer resistances. We recently showed that capacity fade of NCM-based SSBs is closely related to chemo-mechanical effects.[8] Without a fluid or elastic compound, volume changes in solid-state batteries can cause delamination of electrode materials from the SE and crack nucleation occurs. Continuous swelling and contraction during charge and discharge can lead to secondary particle cracking or even electrolyte cracking (depending on the mechanical softness) and thus eventually battery failure.[6–8,17] Similar effects may occur due to local overcharging of particles depending on the electronic and ionic percolation in the electrode. Inhomogeneous stress development may induce further particle cracking. However, not only

View Article Online
DOI: 10.1039/C8EE00907D

the electrode materials but also the separator is affected.[70] Cannarella and Arnold predicted that the ionic conductivity of porous LIB separators is decreased under mechanical stress, an issue that is circumvented in solid-state systems.[71]

Mechanical properties of electrode components: An important parameter that must be considered when evaluating the stress of a solid-state battery system is the softness of the solid electrolyte itself. As the active electrode materials are commonly employed as composites, rather than single-phase materials, stress release of the active materials can partly be compensated by elastic deformation of the SE, depending on its intrinsic stiffness. This stiffness is usually expressed by the Young's modulus (elastic modulus) E, which varies significantly with the type of SE.[72,73] The shear modulus G is an indicator of the stiffness of a material when experiencing shear deformation. According to a model proposed by Monroe and Newman, a SE is required to have a sufficiently high shear modulus of $G > 8.5$ GPa in order to suppress lithium dendrite formation.[74,75] However, this model was originally developed for polymers and is found to be only partially valid for inorganic solids.[76–78] The bulk modulus K is a measure for the compressibility of a solid compound and yields information on the external, hydrostatic pressure that has to be applied to cause a volume change of the material. Another elastic constant is the Poisson's ratio υ which represents the purely kinematic relation of transversal strain to axial strain and is also a measure of the compressibility of the material ($\upsilon = 0.5$ applies for incompressible materials). A list of mechanical properties of common electrode materials compared to state of the art solid electrolytes is given in Table 1. Note that only two constants are necessary to describe an isotropic material uniquely. The presented data were obtained either from nano-indentation and ultrasonic measurement or are theoretical values based on first principle calculations.

View Article Online
DOI: 10.1039/C8EE00907D

Table 1: *Elastic constants of selected SE and electrode materials.*

	Material	Young's Modulus *E*/GPa	Poisson's ratio *υ*	Shear Modulus *G*/GPa	Bulk Modulus *K*/GPa	References
Cathode	$LiCoO_2$	191.0	0.24	80	122.4*	J. Sakamoto[79]
	$LiNi_{0.33}Co_{0.33}Mn_{0.33}O_2$	199.0	0.25	78	132.6*	J. Sakamoto[80]
	$LiFePO_4$†	117.8	0.30	45.5	98.2*	G. Ceder[81]
	$LiMn_2O_4$†	194.0	0.26	77.0	134.7*	K.J. Kim[82]
Solid Electrolytes	$xLi_2S\cdot(100\text{-}x)P_2S_5$	14-23	0.27-0.37	5-9	13-21*	M. Tatsumisago; K.J. Van Vliet[33,83–85]
	γ-Li_3PS_4†	36.9	0.26	14.1	31.9	H. Yan[86]
	β-Li_3PS_4†	28.9	0.27	11.3	21.4	H. Yan[86]
	$Li_{10}GeP_2S_{12}$†	37.2	0.30	14.3	31.0*	C.Y. Ouyang; W.G.Zeier[87,88]
	$Li_7P_3S_{11}$†	21.9	0.36	8.1	23.9	S.P. Ong[89]
	Li_6PS_5X (X = Cl, Br, I)†	22-30	0.33-0.37	8-11	28-30	S.P. Ong[89]
	$Li_7La_3Zr_2O_{12}$ (LLZO)	150.3	0.26	60.0	102.8	J. Wolfenstine; J. Sakamoto; J.D. Siegel[73,90,91]
	Ta-doped LLZO	154.9	0.24	62.5	99.2	J.D. Siegel[73]
	Al-doped LLZO	162.6	0.26	64.6	112.4	J.D. Siegel[73]
	LiPON‡	77.0	0.25	31.0	51.3*	G.M. Pharr[92]
	γ-Li_3PO_4†	103.4	0.26	40.9	72.5	S.P. Ong[89]
	$LiTi_2(PO_4)_3$†	143.7	0.25	57.6	95.0	S.P. Ong[89]
	$NaZr_2(PO_4)_3$†	120.9	0.27	47.7	86.3	S.P. Ong[89]
	$75Na_2S\cdot25P_2S_5$	14.0	0.32	5.3	13.0*	M. Tatsumisago[83]
Anode	Lithium	4.9	0.42	4.2	11.0	L. Kaye; J. Newman; T.H. Laby[75,93,94]
	Indium	12.6	0.45	4.4	42.2	L. Parrini[95]
	$LiTi_2O_4$†	181.0	0.25	73.1	125.1	H.B. Qiao[96]
	Graphite	32.0	0.31	12.0	28.1*	A. Timmons; K.J. Kim[82,97]
	a-Silicon†	96.0	0.29	62.0	90.0	Y. Qi[98]

†Theoretical prediction, *complementary results of calculation based on eq. a1, ‡thin film measurement. Accuracy of the data is given in the references.

Thiophosphate-based SEs have Young's moduli on the order of 20 GPa and are quite elastic ($K/G > 1.75$), with glasses being "softer" than their crystalline counterparts.[33,85,86,99] On the

View Article Online
DOI: 10.1039/C8EE00907D

other hand oxide materials like e.g. LLZO exhibit Young's moduli of 150 GPa or more and are much less elastic.[73] This lower elasticity may increase the risk of fracture of the SE. On the other hand, it has recently been shown that the "softness" of a SE influences the intrinsic ionic transport itself,[100–103] and the pressure influence on the ion transport in soft materials is still unknown. Cathode active materials are usually oxide or phosphate materials and less elastic with rather high Young's moduli compared to most solid electrolytes, which underlines the need for them to be embedded in a more elastic matrix than can sustain and buffer the volume changes during cycling. While LTO can be regarded as a typical rigid oxide material, graphite and, even more, metal electrodes like lithium or indium foil are rather soft. Interestingly, the partial molar volume of Li of anode materials (with LTO being an exception) exceeds that of most CAMs (Figure 2), but together with lower Young´s modulus this leads to a reduced risk of mechanical failure than in the case of CAMs.

It should be noted that first principles calculations also suggest a dependence of the elastic properties on the degree of lithiation, which makes evaluation and use of this data challenging.[82] For example, the Young's modulus of graphite undergoes a threefold increase during lithium intercalation.[97] Similar effects have to be considered for alloying metal electrodes, but data are rarely available.[104]

Operando stress measurements of full cells – formal treatment: The third option to evaluate stress caused by volume changes of electrode materials in solid-state batteries is to monitor the resulting pressure/stress changes of operating cells. The build-up of pressure during discharge/charge of a volume-constrained battery is a direct measure of the combined effect of volume changes during operation and the elasticity (and plasticity; here ignored in the estimates) of the cell. The measured pressure can be compared to the calculated (estimated) data and used to judge the plastic flow in the battery experimentally. Without performing an experiment, a very simple but reasonable first estimation can be made by calculating the linear elastic strain given by the volumetric strain of the active material and the bulk modulus of the SE, K_{SE} (see Supplementary Information):

$$\Delta p = -\varepsilon_{vol} \cdot K \qquad (11)$$

If we assume that the cell is fully constrained and the complete cathode material is electrochemically addressed during charge, we obtain p(LCO/LTO) = 144 bar and p(NCM/LTO) = -659 bar, see supporting information for details of the calculation. For cells having a higher active material fraction, *i.e.* thinner separator, the bulk modulus of the calculation has to be adjusted and is no longer $K \approx K_{SE}$.

View Article Online
DOI: 10.1039/C8EE00907D

In the setup employed here, the battery pellets are fixed in a peek cylinder with steel pistons on the top and bottom of the battery. When cycling the batteries, pressure changes occur due to volume changes of the active materials upon lithium insertion and extraction. This pressure can be measured, as the resulting volume change is mostly translated uniaxially towards the steel stamps. By attaching a force sensor to the setup, the uniaxial stress σ_{11} is monitored *in situ* (see Figure S2). The obtained stress is corrected by the materials mechanical relaxation and hence the net pressure changes for a given electrode configuration can be extracted. By employing a zero-strain anode material as lithium titanate, the net pressure change during galvanostatic cycling can be fully attributed to the volume change from the CAM. The herein investigated CAMs are LCO, NCM-811 and NCA using LTO as counter electrode. Stress measurements of AAMs were conducted for cells using an NCM-811 cathode material, in which the volume expansion is accounted for, for either graphite, lithium metal or indium metal as a counter electrode.

Operando stress measurements of full cells – Experimental results: The electrochemically induced periodic changes of the nominal pressure after subtracting the baseline (an example can be found in the Supplementary Information Figure S5) are shown in Figure 4. As the cells are galvanostatically cycled, the pressure change during charge and discharge can be directly correlated to the degree of lithiation x of the CAM (Figure 4, right column). Upon lithiation, the induced volume change is reversed and the periodically alternating stress can be monitored with cycling. An increase of the current density leads to a lower capacity and consequently the net stress change is lower because less lithium is transferred.

View Article Online
DOI: 10.1039/C8EE00907D

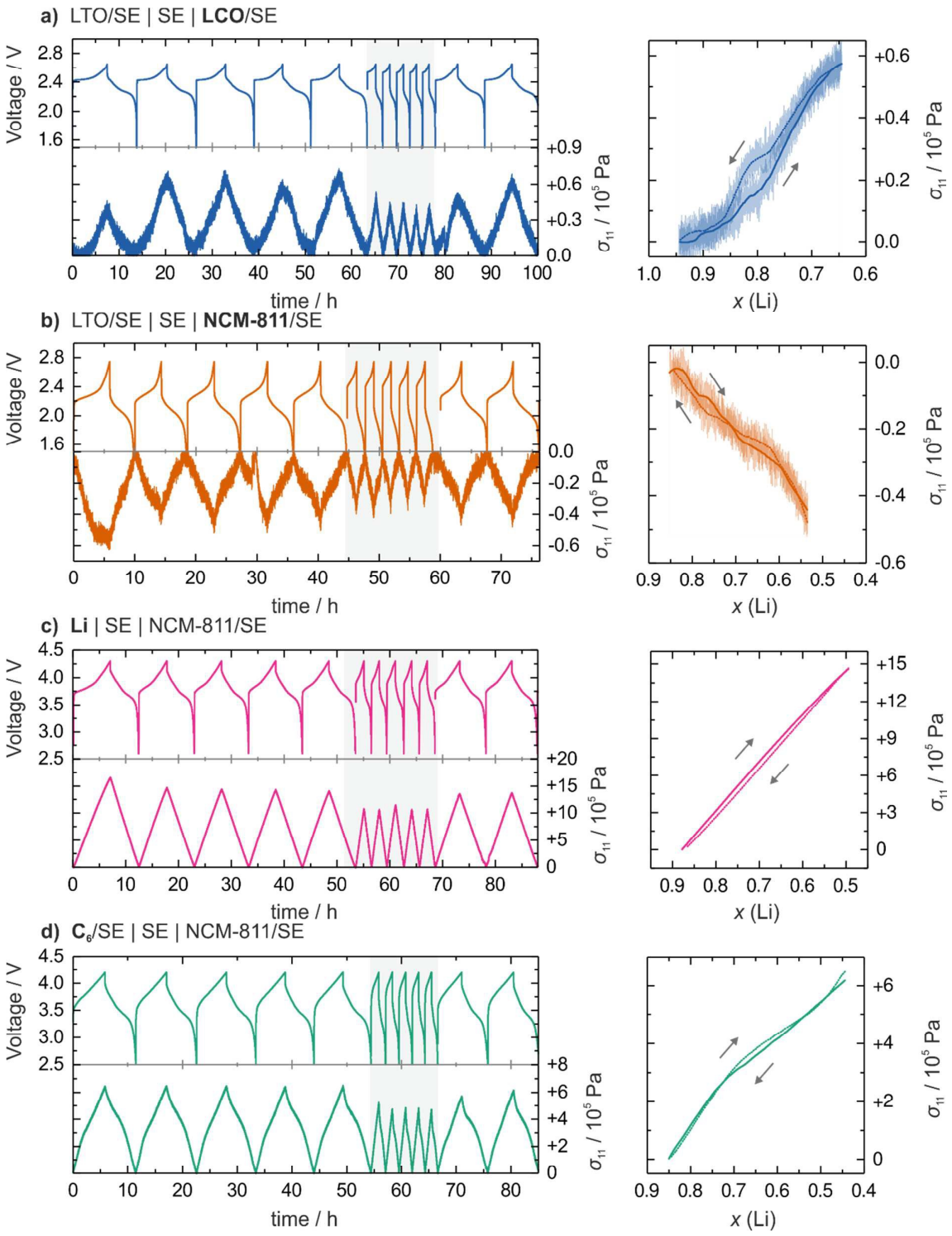

Figure 4: Galvanostatically induced change of the net stress σ_{11} for all-solid-state cells with different electrode configurations. a) LTO/SE | SE | LCO/SE (data from reference[11]), b) LTO/SE | SE | NCM-811/SE, c) Li | SE | NCM-811/SE cell d) LiC_6 | SE | NCM-811/SE. The stress data were corrected by an individual drift to extract the volume expansion of the electrode materials used (left column). From an individual cycle, the stress change can be

View Article Online
DOI: 10.1039/C8EE00907D

correlated to the degree of lithiation of the cathode material (right column). Respective data from (a,b) were smoothed by a Savitzky–Golay filter as a guide to the eye. The solid lines represent the charging curve and the dashed lines the discharge process. The cycling rate is 0.1 C cycle 1 to 5, 0.25 C in cycle 6 to 10 and again 0.1 C in the following cycles. Additional stress measurements for a InLi | SE | NCM/SE cell and a LTO | SE | NCA-801505/SE cell are provided in the Supplementary Information.

In all tested electrode combinations, the pressure changes in a periodic manner, depending on the state of charge (SOC) of the battery. Only the volume effect of LCO is effectively monitored in the cell with the LTO anode (Figure 4a) and the cell volume expands during the charging cycle resulting in a net stress of σ_{11}(LCO/LTO) = +0.6 MPa – which is substantial. In contrast, a negative net pressure of a similar magnitude is observed when NCM-811 is employed in the same setup (Figure 4b). The experiments confirm the effect of the CAM volume change on the battery pressure. When LTO is replaced by a metal anode or graphite (Figure 4c,d), the stress response experiences a ten- to twenty-fold increase, respectively. During the charging process, the anode material is lithiated. The high positive partial molar volume of lithium in e.g. lithium metal or graphite causes a much stronger volume effect on the anode side (see Figure 2b). Is this case, the comparably small effect of the CAM cannot be separated in the net pressure response. The magnitude of the stress caused by the anode materials is significantly higher compared to the observations for CAMs, as suggested by the partial molar volumes given in Figure 2b.

Operando stress measurements on full cells – Interpretation: The experiment of pressure-monitoring during cycling provides information on the linear elastic stress σ_{11} in axial direction, *i.e.* towards the force sensor, but not on the radial components directed to the cylindrical cell casing. However, the results for σ_{11} can be used to derive the respective radial components and approximate the hydrostatic pressure p inside the cell, which is composed of

$$p = -\frac{1}{3}(\sigma_{11} + \sigma_{22} + \sigma_{33}) = \frac{E}{1-2\upsilon}\varepsilon_0. \quad (12)$$

By using a homogenization approach, the effective eigenstrain ε_0 of the battery cell can be estimated. The effective Young 's modulus $E_{\mathrm{Cell}}^{\mathrm{eff}}$ can be obtained by a Reuss approximation.[105] On a cell level, the SE fraction is significantly higher than the fraction of active materials and we can hence assume a Poisson's ratio of $\upsilon_{\mathrm{eff}} = \upsilon(\beta\text{-}Li_3PS_4)$. A detailed description of the model and further parameters are given in the Supplementary Information. The hydrostatic pressure was estimated for the cells LTO/SE | SE | LCO/SE and LTO/SE | SE | NCM-811/SE.

View Article Online
DOI: 10.1039/C8EE00907D

To simplify the model, the anode contribution of the zero-strain LTO was neglected. In doing so, a hydrostatic, compressive pressure of p(LCO/LTO) = 100 bar is calculated, when assuming a volume change ΔV_{cryst}(LCO) = +1.4 % upon delithiation. If nickel-rich NCM, which undergoes a contraction of ΔV_{cryst}(NCM) = -6 %, is used as CAM, the resulting tensile pressure is p(NCM/LTO) = -427 bar. The experiment demonstrates the impact of very small volume changes of the active material components to the cell pressure. Furthermore, the results from the experiment agree very well with the change in hydrostatic pressure from the calculation of the linear strain (see supporting information) – despite the simple formal approach. The experimental values can very well be used as a basis for a more sophisticated 3D approximation.

It has to be taken into account that in a real system, besides not being perfectly constrained, plastic effects will consume some of the locally developed stress. Nevertheless, both, the experiment and the calculation, give insight into the significant pressure/stress arising from very small volume changes of the CAM/AAM. By increasing the energy density of solid-state cells for commercial applications, and inevitably lowering the external force, volume effects of electrode materials will be even more pronounced, of which most of the consequences are yet to be investigated. The stress measurements of SSBs further underline the relevance of the ongoing search for zero-strain electrode materials with practical mean charge/discharge voltages. Application of an external pressure cannot fully compensate delamination of electrode materials. Calculations by Tian *et al.* have shown that re-tightening a cell is not sufficient to recover capacity fade due to contact loss of materials.[30] As lithium metal is desired to serve as a negative electrode material in SSBs, zero volume changes can hardly be achieved; however, reduction is possible by zero-strain cathode material or smart mechanical electrode balancing.[106] Good SSBs may require a minimum porosity in the electrode composites to avoid too strong changes in stress. A certain part of the stress is indeed taken up by the porosity, but this depends critically on the plasticity of the SE. Pore-filling due to volume changes of electrode materials and plastic deformation of SE and electrodes will never work perfectly, as plastic deformation is slow and perhaps not effective enough. Therefore, stress changes will always occur.

Chemo-Mechanical Balancing: To minimize unwanted elastic stress effects, the electrodes need to be optimized with respect to chemical expansion. In order to assess stress effects in operating cells (a) the extent of pore filling due to volume changes and (b) the compressibility of the battery components need to be estimated. The simplest assumption might be that there is always enough pore volume in the composites to take up the stress from the electrode

View Article Online
DOI: 10.1039/C8EE00907D

volume changes. The results for LCO cells show that this is not the case. So, part of the volume change goes into pore filling, part into strain. Additionally, critical particle sizes dependent on the associated volume change of the electrode material have to be considered and may be tailored specifically for solid-state batteries.[107] Nano-sized particles as in the case of silicon can be used to distribute the stress more homogenously in the electrodes and potentially even lower their mean bulk modulus.[108] Another strategy can be the addition of flexible components to the electrodes or electrolyte as shown by Oh and others.[109,110] Similar to conventional LIBs, introduction of e.g. a polymer binder could reduce local stress generation and could counteract crack formation or delamination, which would also be beneficial in terms of industrially processing brittle SEs.

Additionally, mechanically balanced SSBs may combine electrode materials such that a low mean charge and discharge volume is achieved. Anode and cathode should be compatible in this respect, and one may use blending to combine materials with negative and positive chemical expansion. This can either be achieved for the full cell, e.g. NCM and graphite (both with positive partial molar volume of lithium), or within the electrodes themselves, e.g. by combining LCO with NCM (one with negative and one with positive partial molar volume of lithium). The latter is experimentally proven here by cycling a battery using an active material blend of NCM and LCO in a weight ratio of 55:45 %. Figure 5 shows the charge and discharge curves for SSBs using β-Li_3PS_4 and LTO as SE and anode, respectively.

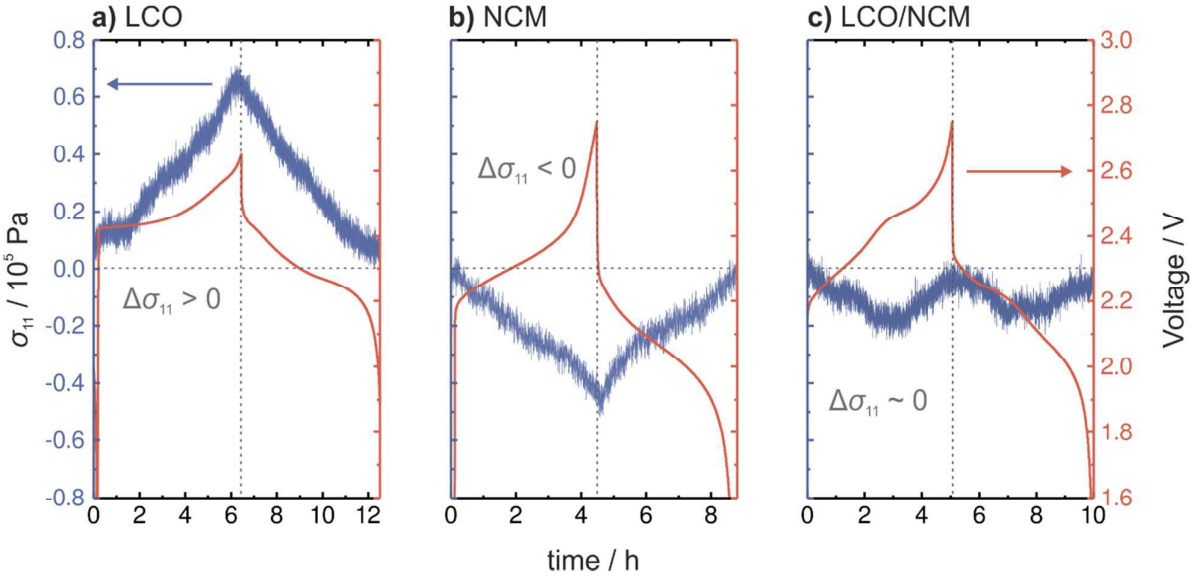

View Article Online
DOI: 10.1039/C8EE00907D

Figure 5: Approach of stress mitigation by cathode active materials balancing. Designing a composite cathode out of a stoichiometric blend of one expanding and one contracting material upon delithiation, will result in stress compensation. Comparison of the stress response of LTO/SE | SE | CAM/SE using a) LCO, b) NCM-811 and c) a blend of 55:45 wt% NCM-811:LCO cathode composite. The cell using LCO exhibits a positive volume expansion, the cell containing NCM-811 shows a negative stress response. However, the cell using the blend shows an overall lower nominal stress. The pressure profile thereby combines the individual profiles of the single cathode materials.

As shown in Figure 2, LCO exhibits a positive and NCM-811 a negative nominal stress change during cycling. The battery employing the blended CAM composite cathode shows a two-step voltage profile which is the combined shape of the voltage curves for the single materials. Similar observations were made in the stress measurement, as the net stress change of the battery resembles the sum of the two opposing stress responses for LCO and NCM-811, resulting in a reduced nominal stress. During charge, the reaction volume change of the material can be partially compensated resulting in a lowered net volume change. The stress generated inside the battery cathode is thus reduced. Overall, we propose this method of *stress optimized cathode composites* to reduce the stress generation in SSBs and minimize the contact loss due to volume changes of the active materials. The advantage of this method is further underlined by a good preservation of the contact between particles of the active materials after cycling, as shown in complimentary SEM and EDX results (Figure S7). A delamination of the active materials from the SE is not observed as recently shown for single CAM cathodes (compare to Figure S8).[88] A combination of anode and cathode or electrode materials within the same electrode can reduce the internal stress of a battery, avoid mechanically induced capacity fading and thus increase the overall electrochemical performance.

5. Conclusion

In this work we emphasize the critical role of volume change of electrode materials in an all-solid-state battery environment. The vast majority of lithium storage electrodes undergo volumetric changes upon lithium insertion/extraction. From a mechanical point of view, particularly the large volumetric strain of the lithium metal anode will be challenging to compensate by cell packing and may even require some kind of mechanical formation step. Further, when considering smaller volume changes, the stress and strain build up in the

View Article Online
DOI: 10.1039/C8EE00907D

electrodes can cause particle cracking, electrode fracture and thus battery deformation. Consequently, using an unfavorable combination of electrode materials and solid electrolytes with regard to volumetric changes and mechanical material properties, e.g. hardness and elasticity, may be detrimental to the battery performance in a solid-state system. Here we present three different techniques to obtain quantitative conclusions on the volume change of electrode materials. *Operando* X-ray diffraction is used to obtain the crystallographic volume change of single materials; however, plasticity, deformation or combinatory effects of the electrode materials are neglected. In particular, plasticity of the solid-electrolyte has to be considered in future studies, as this component needs to compensate volume changes of the electrode materials. An important aspect is the reversibility of the deformation to avoid dead space and high internal transfer resistances by cracks and voids, as this will result in electrochemical isolation of active materials. Stress measurements of operating cells consider the plasticity effects and deformation of the battery materials and represent a more realistic response of the battery performance. However, the stress response is unique to the chosen solid electrolyte(s) and electrode combination(s) and is determined by microstructure, processing and homogeneity of the materials. With respect to solid-state battery development for electric vehicles, there will always be an additional materials' tradeoff between elastic and flexible components and withstanding of mechanical shocks in case of a collision. Thus, the selection of battery components has also to be tailored toward the desired application with respect to the mechanical properties of the materials. In the future, more attention should be directed to the study of (chemo-)mechanical properties of solid-state battery components, as well as their particular combination. This can be particularly supported by developing advanced computational models, which consider the volumetric change and mechanical parameters of solid electrolytes and active materials.

Experimental Methods

Cell assembly.

The crystalline solid electrolyte β-Li_3PS_4 and the electrode materials NCM-811, NCA-801505, graphite and lithium titanate ($Li_4Ti_5O_{12}$) were provided by BASF SE. $LiCoO_2$ was commercially obtained from Alfa Aesar (97 %) and surface coated with a $LiNb_{0.5}Ta_{0.5}O_3$ film using a sol-gel route. The description of the coating process can be found elsewhere.[66] The solid electrolyte $Li_{10}GeP_2S_{12}$ (LGPS) was synthesized by a solid-state route following a previously reported procedure.[66] Prior to use, all powders were dried in a vacuum Büchi oven

View Article Online
DOI: 10.1039/C8EE00907D

at 250 °C overnight and stored in an argon-filled glovebox (H_2O < 0.1 ppm and O_2 < 0.1 ppm). SSBs for monitoring the stress *in operando* were built in a custom cell casing. Cells were assembled following the previously described procedure.[8,66,111]

The composite electrodes were prepared by hand-mixing of the pristine materials. Positive electrode composites (LCO, NCM, NCA) were blended with β-Li_3PS_4 in a mass ratio of 70:30. The composite used for stress mitigation also used 70 wt% of active material, *i.e.* NCM-811 and LCO in a mass ratio of 55:45 by weight. This resulted in an overall composition of NCM-811:LCO:SE of 38:32:30 wt%. The composite was prepared from the single components by hand-mixing in the same manner as for the single component electrodes. Composites for the negative electrodes had a mass ratio of active materials to SE of 35:65 for $Li_4Ti_5O_{12}$ and 50:50 for graphite, respectively. All composite powders were ground in an agate mortar for 15 minutes before assembling the cell. In the case of metal electrodes, a 6 mm diameter indium foil (Alfa Aesar) or lithium foil (Rockwood lithium) were used.

On the positive electrode side, 12 mg of the respective composite cathode powder were used. mass of 60 mg of the sulfide electrolyte served as a separator, corresponding to a thickness of ~400 µm. For the negative electrode, 35 mg of the LTO/SE composite or 12 mg or the graphite/SE composite were employed. Cells only consisting of electrodes in powder form were compressed after full assembly at 35 kN (approximately 445 Mpa). For cells using metal foil electrodes, the powders were compressed at 35 kN prior to addition of the negative electrode. During electrochemical experiments, a reduced pressure of approximately 70 MPa was applied. Details for the cell preparation of pouch cells for *operando* XRD can be found in previous studies.[35,112]

***Operando* X-ray diffraction.** XRD measurements for determination of the unit cell volume change of NCM, NCA and LCO were conducted using a custom diffractometer with Mo-$K_{\alpha 1,2}$ radiation. XRD patterns were collected on pouch cells cycled at 0.1 C at 25 °C. A more detailed description of the experimental setup, cell preparation and data evaluation can be found in previous publications.[35,36,112]

Stress monitoring in operating cells. Stress measurements during galvanostatic cycling were conducted in a modified version of the in-house developed solid-state battery cell as described elsewhere.[8,66] The outer frame was extended and a force sensor (KMT 55, Inelta Sensorsysteme GmbH & Co. KG, Ottobrunn/Munich) was integrated on the bottom side of the cell. The sensor was attached to the bottom steel piston of the battery setup. This allows to adjust a certain strain during battery cycling as well as to monitor the uniaxial stress response

View Article Online
DOI: 10.1039/C8EE00907D

of cell given by the nominal change in force. The cells were oriented so that the monitored electrode was directed to the force sensor. The frame was tightening using a 10 Nm torque, corresponding to a force of 60 ± 8 MPa.

A detailed schematic of the device can be found in the Supplementary Information (Figure S2). The force data was collected by an in-house developed program based on the National Instruments LabVIEW software (Version 11.0.1). All-solid-state cells for stress monitoring were galvanostatically cycled in a temperature-controlled environment at 25 °C.

Battery cycling was carried out on an SP-300 potentiostat/galvanostat (Bio-Logic Science Instruments). NCM, NCA and mixed CAM composites of NCM and LCO, for strain mitigation, were cycled to an upper cutoff voltage of 4.3 V vs. Li^+/Li. For cathodes employing only LCO as an active material, the voltage was adjusted to 4.2 V vs. Li^+/Li. Voltage windows were calculated based on the chosen anode material. The voltage of the negative anode was assumed to be 0.6 V vs. Li^+/Li for indium foil, 1.55 V vs. Li^+/Li for lithium titanate and 0.10 V vs. Li^+/Li for graphite, respectively.[113,114] For cells employing stress mitigating composites using a combination of both, NCM and LCO, the voltage window was set to 1 – 2.75 V (LTO anode) and the current density was adjusted to 186 µA/cm². The selected test procedure for *operando* stress measurements includes 5 cycles at 0.1 C, 5 cycles at 0.25 C followed by open end cycling at 0.1 C. The electrochemical data were then matched to the recorded strain change. Cells were kept at OCV for 20 h prior to cycling to minimize drifts arising from the cell casing (see Supplementary Information). The nominal stress was calculated by subtracting a manually drawn baseline to further reduce contributions from a mechanical drift and subtract the constantly applied force (example can be found in the Supporting Information Figure S3). For the representation of stress changes versus the calculated data (estimated from the theoretical capacity of the cathode materials) for NCM, NCA and LCO were additionally smoothed using a Savitzky-Golay smoothing filter to indicate the trend.

Pressure dependent OCV tests. All pressure dependent OCV measurements were carried out in a custom setup at 25 °C.[115] The uniaxial mechanical stress exerted at the top of SSB pellets was monitored by a pressure gauge at the bottom of the cell. The cell assembly procedure is the same as described before.[11] SSBs were charged under galvanostatic conditions at 0.1C (*i.e.* 90 µA for the InLi | LGPS | LCO/LGPS cell and 140 µA for the InLi | LGPS | LTO/LGPS cell). The pressure was set to 0.5 t during charge. Pressure dependent OCV tests were carried out at various states-of-charge (SOC). After each charging step, cells rested until a stable OCV (with voltage drop < ~0.005 V/s) was obtained. Then, the

View Article Online
DOI: 10.1039/C8EE00907D

OCV was recorded at 5 different pressures: 0.5 t – 1.2 t – 1.7 t – 2.2 t – 2.8 t (55 MPa – 94 MPa – 143 MPa– 192 MPa). The procedure is repeated until the cell is fully charged to the set upper cutoff voltage (see Supporting Information).

Scanning electron microscopy and energy dispersive X-ray analysis. Microstructure images of the cathodes extracted from disassembled cells were obtained on a Merlin high-resolution scanning electron microscope (Carl Zeiss AG, Germany). The samples were transferred from a glove box in the analysis chamber under argon atmosphere using a transfer vessel (Leica EM VC500). EDX analysis was conducted using an XMAX EXTREME EDX detector (Oxford Instruments, United Kingdom). Measurements were carried out by application of an acceleration voltage of 5 kV and a probing current of 100 pA for SEM and 1000 pA for EDX.

View Article Online
DOI: 10.1039/C8EE00907D

Supplemental Information

OCV of an InLi | SE | LTO and a LCO| SE | InLi cell upon increasing the cell pressure. Schematic of the setup for monitoring the pressure change in operating cells. Reuss approximation for the estimation of the hydrostatic pressure inside an SSBs. Stress measurements of NCA | SE | LTO and InLi | SE | NCM-811, SEM/EDX analysis of disassembled CAM composite electrodes

AUTHOR INFORMATION

Corresponding Authors

*wolfgang.g.zeier@phys.chemie.uni-giessen.de; *juergen.janek@phys.chemie.uni-giessen.de

Notes

The authors declare no competing financial interests.

Acknowledgements

The authors acknowledge financial support by BASF SE within the International Network for Electrochemistry and Batteries. R.K. acknowledges support by the Funds of the Chemical Industry (FCI). The authors thank H. Weigand for development of the measurement apparatus for operando pressure measurements and for conceptional drawings. The authors thank W. Koerver for development of the LabView environment for stress measurements. The authors thank I. Aygün for her help in cell preparation.

References

(1) Mukhopadhyay, A.; Sheldon, B. W. Deformation and Stress in Electrode Materials for Li-Ion Batteries. *Prog. Mater. Sci.* **2014**, *63*, 58–116.

(2) Koyama, Y.; Chin, T. E.; Rhyner, U.; Holman, R. K.; Hall, S. R.; Chiang, Y. M. Harnessing the Actuation Potential of Solid-State Intercalation Compounds. *Adv. Funct. Mater.* **2006**, *16*, 492–498.

(3) Mukhopadhyay, A.; Guo, F.; Tokranov, A.; Xiao, X.; Hurt, R. H.; Sheldon, B. W. Engineering of Graphene Layer Orientation to Attain High Rate Capability and Anisotropic Properties in Li-Ion Battery Electrodes. *Adv. Funct. Mater.* **2013**, *23*, 2397–2404.

(4) Mukhopadhyay, A.; Tokranov, A.; Xiao, X.; Sheldon, B. W. Stress Development Due to Surface Processes in Graphite Electrodes for Li-Ion Batteries: A First Report. *Electrochim.*

View Article Online
DOI: 10.1039/C8EE00907D

Acta **2012**, *66*, 28–37.

(5) Tokranov, A.; Sheldon, B. W.; Lu, P.; Xiao, X.; Mukhopadhyay, A. The Origin of Stress in the Solid Electrolyte Interphase on Carbon Electrodes for Li Ion Batteries. *J. Electrochem. Soc.* **2013**, *161*, A58–A65.

(6) Shearing, P. R. Batteries: Imaging Degradation. *Nat. Energy* **2016**, *1*, 16173.

(7) Sun, G.; Sui, T.; Song, B.; Zheng, H.; Lu, L.; Korsunsky, A. M. On the Fragmentation of Active Material Secondary Particles in Lithium Ion Battery Cathodes Induced by Charge Cycling. *Extrem. Mech. Lett.* **2016**, *9*, 449–458.

(8) Koerver, R.; Aygün, I.; Leichtweiß, T.; Dietrich, C.; Zhang, W.; Binder, J. O.; Hartmann, P.; Zeier, W. G.; Janek, J. Capacity Fade in Solid-State Batteries: Interphase Formation and Chemomechanical Processes in Nickel-Rich Layered Oxide Cathodes and Lithium Thiophosphate Solid Electrolytes. *Chem. Mater.* **2017**, *29*, 5574–5582.

(9) Robert, R.; Novak, P. Structural Changes and Microstrain Generated on $LiNi_{0.80}Co_{0.15}Al_{0.05}O_2$ during Cycling: Effects on the Electrochemical Performance. *J. Electrochem. Soc.* **2015**, *162*, A1823–A1828.

(10) Janek, J.; Zeier, W. G. A Solid Future for Battery Development. *Nat. Energy* **2016**, *1*, 16141.

(11) Zhang, W.; Schröder, D.; Arlt, T.; Manke, I.; Koerver, R.; Pinedo, R.; Weber, D. A.; Sann, J.; Zeier, W. G.; Janek, J. (Electro)Chemical Expansion during Cycling: Monitoring the Pressure Changes in Operating Solid-State Lithium Batteries. *J. Mater. Chem. A* **2017**, *5*, 9929–9936.

(12) Aurbach, D.; Zinigrad, E.; Cohen, Y.; Teller, H. A Short Review of Failure Mechanisms of Lithium Metal and Lithiated Graphite Anodes in Liquid Electrolyte Solutions. *Solid State Ionics* **2002**, *148*, 405–416.

(13) Ito, S.; Fujiki, S.; Yamada, T.; Aihara, Y.; Park, Y.; Kim, T. Y.; Baek, S.-W.; Lee, J.-M.; Doo, S.; Machida, N. A Rocking Chair Type All-Solid-State Lithium Ion Battery Adopting Li_2O–ZrO_2 Coated $LiNi_{0.8}Co_{0.15}Al_{0.05}O_2$ and a Sulfide Based Electrolyte. *J. Power Sources* **2014**, *248*, 943–950.

(14) Ohzuku, T.; Ueda, A.; Yamamoto, N.; Iwakoshi, Y. Factor Affecting the Capacity Retention of Lithium-Ion Cells. *J. Power Sources* **1995**, *54*, 99–102.

(15) Vetter, J.; Novák, P.; Wagner, M. R.; Veit, C.; Möller, K. C.; Besenhard, J. O.; Winter, M.; Wohlfahrt-Mehrens, M.; Vogler, C.; Hammouche, A. Ageing Mechanisms in Lithium-Ion Batteries. *J. Power Sources* **2005**, *147*, 269–281.

(16) Chin, T. E.; Rhyner, U.; Koyama, Y.; Hall, S. R.; Chiang, Y.-M. Lithium Rechargeable Batteries as Electromechanical Actuators. *Electrochem. Solid-State Lett.* **2006**, *9*, A134–A138.

(17) Fu, R.; Xiao, M.; Choe, S. Y. Modeling, Validation and Analysis of Mechanical Stress Generation and Dimension Changes of a Pouch Type High Power Li-Ion Battery. *J. Power Sources* **2013**, *224*, 211–224.

(18) Cannarella, J.; Arnold, C. B. State of Health and Charge Measurements in Lithium-Ion Batteries Using Mechanical Stress. *J. Power Sources* **2014**, *269*, 7–14.

(19) Ebner, M.; Marone, F.; Stampanoni, M.; Wood, V. Visualization and Quantification of Electrochemical and Mechanical Degradation in Li Ion Batteries. *Science* **2013**, *342*, 716–720.

(20) Oh, K. Y.; Samad, N. A.; Kim, Y.; Siegel, J. B.; Stefanopoulou, A. G.; Epureanu, B. I. A Novel Phenomenological Multi-Physics Model of Li-Ion Battery Cells. *J. Power Sources* **2016**, *326*, 447–458.

(21) Luo, J.; Dai, C. Y.; Wang, Z.; Liu, K.; Mao, W. G.; Fang, D. N.; Chen, X. In-Situ Measurements of Mechanical and Volume Change of $LiCoO_2$ Lithium-Ion Batteries during

View Article Online
DOI: 10.1039/C8EE00907D

Repeated Charge–discharge Cycling by Using Digital Image Correlation. *Measurement* **2016**, *94*, 759–770.

(22) Zhang, N.; Tang, H. Dissecting Anode Swelling in Commercial Lithium-Ion Batteries. *J. Power Sources* **2012**, *218*, 52–55.

(23) Dai, K.; Wang, Z.; Ai, G.; Zhao, H.; Yuan, W.; Song, X.; Battaglia, V.; Sun, C.; Wu, K.; Liu, G. The Transformation of Graphite Electrode Materials in Lithium-Ion Batteries after Cycling. *J. Power Sources* **2015**, *298*, 349–354.

(24) Taminato, S.; Yonemura, M.; Shiotani, S.; Kamiyama, T.; Torii, S.; Nagao, M.; Ishikawa, Y.; Mori, K.; Fukunaga, T.; Onodera, Y.; et al. Real-Time Observations of Lithium Battery Reactions—operando Neutron Diffraction Analysis during Practical Operation. *Sci. Rep.* **2016**, *6*, 28843.

(25) Ishidzu, K.; Oka, Y.; Nakamura, T. Lattice Volume Change during Charge/Discharge Reaction and Cycle Performance of $Li[Ni_xCo_yMn_z]O_2$. *Solid State Ionics* **2016**, *288*, 176–179.

(26) Wang, D.; Wu, X.; Wang, Z.; Chen, L. Cracking Causing Cyclic Instability of $LiFePO_4$ Cathode Material. *J. Power Sources* **2005**, *140*, 125–128.

(27) Sakuda, A.; Takeuchi, T.; Kobayashi, H. Electrode Morphology in All-Solid-State Lithium Secondary Batteries Consisting of $LiNi_{1/3}Co_{1/3}Mn_{1/3}O_2$ and Li_2S-P_2S_5 Solid Electrolytes. *Solid State Ionics* **2016**, *285*, 112–117.

(28) Wang, H.; Jang, Y.-I.; Huang, B.; Sadoway, D. R.; Chiang, Y.-M. TEM Study of Electrochemical Cycling-Induced Damage and Disorder in $LiCoO_2$ Cathodes for Rechargeable Lithium Batteries. *J. Electrochem. Soc.* **1999**, *146*, 473–480.

(29) Yamakawa, S.; Nagasako, N.; Yamasaki, H.; Koyama, T.; Asahi, R. Phase-Field Modeling of Stress Generation in Polycrystalline $LiCoO_2$. *Solid State Ionics* **2018**, *319*, 209–217.

(30) Tian, H.-K.; Qi, Y. Simulation of the Effect of Contact Area Loss in All-Solid-State Li-Ion Batteries. *J. Electrochem. Soc.* **2017**, *164*, E3512–E3521.

(31) Korte, C.; Keppner, J.; Peters, A.; Schichtel, N.; Aydin, H.; Janek, J. Coherency Strain and Its Effect on Ionic Conductivity and Diffusion in Solid Electrolytes – an Improved Model for Nanocrystalline Thin Films and a Review of Experimental Data. *Phys. Chem. Chem. Phys.* **2014**, *16*, 24575–24591.

(32) Schichtel, N.; Korte, C.; Hesse, D.; Janek, J. Elastic Strain at Interfaces and Its Influence on Ionic Conductivity in Nanoscaled Solid Electrolyte Thin Films—theoretical Considerations and Experimental Studies. *Phys. Chem. Chem. Phys.* **2009**, *11*, 3043.

(33) Sakuda, A.; Hayashi, A.; Tatsumisago, M. Sulfide Solid Electrolyte with Favorable Mechanical Property for All-Solid-State Lithium Battery. *Sci. Rep.* **2013**, *3*, 2261.

(34) Bucci, G.; Swamy, T.; Chiang, Y.-M.; Carter, W. C. Modeling of Internal Mechanical Failure of All-Solid-State Batteries during Electrochemical Cycling, and Implications for Battery Design. *J. Mater. Chem. A* **2017**, *5*, 19422–19430.

(35) Kondrakov, A. O.; Schmidt, A.; Xu, J.; Geßwein, H.; Mönig, R.; Hartmann, P.; Sommer, H.; Brezesinski, T.; Janek, J. On the Anisotropic Lattice Strain and Mechanical Degradation of High- and Low-Nickel NCM Cathode Materials for Li-Ion Batteries. *J. Phys. Chem. C* **2017**, *121*, 3286–3294.

(36) Schweidler, S.; de Biasi, L.; Schiele, A.; Hartmann, P.; Brezesinski, T.; Janek, J. Volume Changes of Graphite Anodes Revisited: A Combined Operando X-Ray Diffraction and In Situ Pressure Analysis Study. *J. Phys. Chem. C* **2018**, *122*, 8829–8835.

(37) de Biasi, L.; Kondrakov, A. O.; Geßwein, H.; Brezesinski, T.; Hartmann, P.; Janek, J. Between Scylla and Charybdis: Balancing Among Structural Stability and Energy Density of Layered

View Article Online
DOI: 10.1039/C8EE00907D

NCM Cathode Materials for Advanced Lithium-Ion Batteries. *J. Phys. Chem. C* **2017**, *121*, 26163–26171.

(38) Yamada, A.; Koizumi, H.; Sonoyama, N.; Kanno, R. Phase Change in Li_xFePO_4. *Electrochem. Solid-State Lett.* **2005**, *8*, A409–A413.

(39) Sauerteig, D.; Ivanov, S.; Reinshagen, H.; Bund, A. Reversible and Irreversible Dilation of Lithium-Ion Battery Electrodes Investigated by in-Situ Dilatometry. *J. Power Sources* **2017**, *342*, 939–946.

(40) Wilkinson, D. P.; Wainwright, D. In-Situ Study of Electrode Stack Growth in Rechargeable Cells at Constant Pressure. *J. Electroanal. Chem.* **1993**, *355*, 193–203.

(41) Rieger, B.; Erhard, S. V.; Rumpf, K.; Jossen, A. A New Method to Model the Thickness Change of a Commercial Pouch Cell during Discharge. *J. Electrochem. Soc.* **2016**, *163*, A1566–A1575.

(42) Reimers, J. N. Electrochemical and In Situ X-Ray Diffraction Studies of Lithium Intercalation in Li_xCoO_2. *J. Electrochem. Soc.* **1992**, *139*, 2091–2097.

(43) Buchberger, I.; Seidlmayer, S.; Pokharel, A.; Piana, M.; Hattendorff, J.; Kudejova, P.; Gilles, R.; Gasteiger, H. A. Aging Analysis of Graphite/$LiNi_{1/3}Mn_{1/3}Co_{1/3}O_2$ Cells Using XRD, PGAA, and AC Impedance. *J. Electrochem. Soc.* **2015**, *162*, 2737–2746.

(44) Li, J.; Downie, L. E.; Ma, L.; Qiu, W.; Dahn, J. R. Study of the Failure Mechanisms of $LiNi_{0.8}Mn_{0.1}Co_{0.1}O_2$ Cathode Material for Lithium Ion Batteries. *J. Electrochem. Soc.* **2015**, *162*, 1401–1408.

(45) Ghanty, C.; Markovsky, B.; Erickson, E. M.; Talianker, M.; Haik, O.; Tal-Yossef, Y.; Mor, A.; Aurbach, D.; Lampert, J.; Volkov, A.; et al. Li^+-Ion Extraction/Insertion of Ni-Rich $Li_{1+x}(Ni_yCo_zMn_z)_wO_2$ ($0.005< x <0.03$; Y : Z =8:1, w ≈1) Electrodes: In Situ XRD and Raman Spectroscopy Study. *ChemElectroChem* **2015**, *2*, 1479–1486.

(46) Van der Ven, A.; Aydinol, M. K.; Ceder, G.; Kresse, G.; Hafner, J. First-Principles Investigation of Phase Stability in Li_xCoO_2. *Phys. Rev. B* **1998**, *58*, 2975–2987.

(47) Laubach, S.; Laubach, S.; Schmidt, P. C.; Ensling, D.; Schmid, S.; Jaegermann, W.; Thißen, A.; Nikolowski, K.; Ehrenberg, H. Changes in the Crystal and Electronic Structure of LiCoO2 and LiNiO2 upon Li Intercalation and De-Intercalation. *Phys. Chem. Chem. Phys.* **2009**, *11*, 3278.

(48) Liang, C.; Longo, R. C.; Kong, F.; Zhang, C.; Nie, Y.; Zheng, Y.; Kim, J. S.; Jeon, S.; Choi, S. A.; Cho, K. Obstacles toward Unity Efficiency of $LiNi_{1-2x}Co_xMn_xO_2$ ($x = 0 \sim 1/3$) (NCM) Cathode Materials: Insights from Ab Initio Calculations. *J. Power Sources* **2017**, *340*, 217–228.

(49) Li, J.; Petibon, R.; Glazier, S.; Sharma, N.; Pang, W. K.; Peterson, V. K.; Dahn, J. R. In-Situ Neutron Diffraction Study of a High Voltage $Li(Ni_{0.42}Mn_{0.42}Co_{0.16})O_2$/Graphite Pouch Cell. *Electrochim. Acta* **2015**, *180*, 234–240.

(50) Li, J.; Shunmugasundaram, R.; Doig, R.; Dahn, J. R. In Situ X-Ray Diffraction Study of Layered Li-Ni-Mn-Co Oxides: Effect of Particle Size and Structural Stability of Core-Shell Materials. *Chem. Mater.* **2016**, *28*, 162–171.

(51) Ryu, I.; Choi, J. W.; Cui, Y.; Nix, W. D. Size-Dependent Fracture of Si Nanowire Battery Anodes. *J. Mech. Phys. Solids* **2011**, *59*, 1717–1730.

(52) Winter, M.; Besenhard, J. O.; Spahr, M. E.; Novák, P. Insertion Electrode Materials for Rechargeable Lithium Batteries. *Adv. Mater.* **1998**, *10*, 725–763.

(53) Ohzuku, T.; Iwakoshi, Y.; Sawai, K. Formation of Lithium-Graphite Intercalation Compounds in Nonaqueous Electrolytes and Their Application as a Negative Electrode for a Lithium Ion

View Article Online
DOI: 10.1039/C8EE00907D

(Shuttlecock) Cell. *J. Electrochem. Soc.* **1993**, *140*, 2490.

(54) Dahn, J. R. Phase Diagram of Li_xC_6. *Phys. Rev. B* **1991**, *44*, 9170–9177.

(55) Ohzuku, T.; Ueda, A.; Yamamoto, N. Zero-Strain Insertion Material of $Li[Li_{1/3}Ti_{5/3}]O_4$ for Rechargeable Lithium Cells. *J. Electrochem. Soc.* **1995**, *142*, 1431–1435.

(56) Ferg, E.; Gummow, R. J.; Kock, A. De. Spinel Anodes for Lithium-Ion Batteries. *J. Electrochem. Soc.* **1994**, *141*, 9–12.

(57) Meethong, N.; Huang, H. Y. S.; Speakman, S. A.; Carter, W. C.; Chiang, Y. M. Strain Accommodation during Phase Transformations in Olivine-Based Cathodes as a Materials Selection Criterion for High-Power Rechargeable Batteries. *Adv. Funct. Mater.* **2007**, *17*, 1115–1123.

(58) Wang, J. W.; He, Y.; Fan, F.; Liu, X. H.; Xia, S.; Liu, Y.; Harris, C. T.; Li, H.; Huang, J. Y.; Mao, S. X.; et al. Two-Phase Electrochemical Lithiation in Amorphous Silicon. *Nano Lett.* **2013**, *13*, 709–715.

(59) Loveridge, M. J.; Lain, M. J.; Johnson, I. D.; Roberts, A.; Beattie, S. D.; Dashwood, R.; Darr, J. A.; Bhagat, R. Towards High Capacity Li-Ion Batteries Based on Silicon-Graphene Composite Anodes and Sub-Micron V-Doped $LiFePO_4$ Cathodes. *Sci. Rep.* **2016**, *6*, 37787.

(60) de Biasi, L.; Lieser, G.; Dräger, C.; Indris, S.; Rana, J.; Schumacher, G.; Mönig, R.; Ehrenberg, H.; Binder, J. R.; Geßwein, H. $LiCaFeF_6$: A Zero-Strain Cathode Material for Use in Li-Ion Batteries. *J. Power Sources* **2017**, *362*, 192–201.

(61) You, Y.; Wu, X.-L.; Yin, Y.-X.; Guo, Y.-G. A Zero-Strain Insertion Cathode Material of Nickel Ferricyanide for Sodium-Ion Batteries. *J. Mater. Chem. A* **2013**, *1*, 14061–14065.

(62) Mukai, K.; Kato, Y.; Nakano, H. Understanding the Zero-Strain Lithium Insertion Scheme of $Li[Li_{1/3}Ti_{5/3}]O_4$: Structural Changes at Atomic Scale Clarified by Raman Spectroscopy. *J. Phys. Chem. C* **2014**, *118*, 2992–2999.

(63) Guggenheim, E. A. Thermodynamics: An Advanced Treatment for Chemists and Physicists. **1959**.

(64) Wenzel, S.; Randau, S.; Leichtweiß, T.; Weber, D. A.; Sann, J.; Zeier, W. G.; Janek, J. Direct Observation of the Interfacial Instability of the Fast Ionic Conductor $Li_{10}GeP_2S_{12}$ at the Lithium Metal Anode. *Chem. Mater.* **2016**, *28*, 2400–2407.

(65) Zhang, W.; Leichtweiß, T.; Culver, S. P.; Koerver, R.; Das, D.; Weber, D. A.; Zeier, W. G.; Janek, J. The Detrimental Effects of Carbon Additives in $Li_{10}GeP_2S_{12}$ -Based Solid-State Batteries. *ACS Appl. Mater. Interfaces* **2017**, *9*, 35888–35896.

(66) Zhang, W.; Weber, D. A.; Weigand, H.; Arlt, T.; Manke, I.; Schröder, D.; Koerver, R.; Leichtweiss, T.; Hartmann, P.; Zeier, W. G.; et al. Interfacial Processes and Influence of Composite Cathode Microstructure Controlling the Performance of All-Solid-State Lithium Batteries. *ACS Appl. Mater. Interfaces* **2017**, *9*, 17835–17845.

(67) Christensen, J.; Newman, J. A Mathematical Model of Stress Generation and Fracture in Lithium Manganese Oxide. *J. Electrochem. Soc.* **2006**, *153*, A1019–A1030.

(68) Christensen, J.; Newman, J. Stress Generation and Fracture in Lithium Insertion Materials. *J. Solid State Electrochem.* **2006**, *10*, 293–319.

(69) Meethong, N.; Huang, H.-Y. S.; Carter, W. C.; Chiang, Y.-M. Size-Dependent Lithium Miscibility Gap in Nanoscale $Li_{1-x}FePO_4$. *Electrochem. Solid-State Lett.* **2007**, *10*, A134–A138.

(70) Peabody, C.; Arnold, C. B. The Role of Mechanically Induced Separator Creep in Lithium-Ion Battery Capacity Fade. *J. Power Sources* **2011**, *196*, 8147–8153.

(71) Cannarella, J.; Arnold, C. B. Ion Transport Restriction in Mechanically Strained Separator

View Article Online
DOI: 10.1039/C8EE00907D

Membranes. *J. Power Sources* **2013**, *226*, 149–155.

(72) Sakanoi, R.; Shimazaki, T.; Xu, J.; Higuchi, Y.; Ozawa, N.; Sato, K.; Hashida, T.; Kubo, M. Communication: Different Behavior of Young's Modulus and Fracture Strength of CeO_2: Density Functional Theory Calculations. *J. Chem. Phys.* **2014**, *140*, 121102.

(73) Yu, S.; Schmidt, R. D.; Garcia-Mendez, R.; Herbert, E.; Dudney, N. J.; Wolfenstine, J. B.; Sakamoto, J.; Siegel, D. J. Elastic Properties of the Solid Electrolyte $Li_7La_3Zr_2O_{12}$ (LLZO). *Chem. Mater.* **2016**, *28*, 197–206.

(74) Monroe, C.; Newman, J. The Effect of Interfacial Deformation on Electrodeposition Kinetics. *J. Electrochem. Soc.* **2004**, *151*, A880–A886.

(75) Monroe, C.; Newman, J. The Impact of Elastic Deformation on Deposition Kinetics at Lithium/Polymer Interfaces. *J. Electrochem. Soc.* **2005**, *152*, A396–A404.

(76) Porz, L.; Swamy, T.; Sheldon, B. W.; Rettenwander, D.; Frömling, T.; Thaman, H. L.; Berendts, S.; Uecker, R.; Carter, W. C.; Chiang, Y.-M. M. Mechanism of Lithium Metal Penetration through Inorganic Solid Electrolytes. *Adv. Energy Mater.* **2017**, *7*, 1–12.

(77) Cheng, E. J.; Sharafi, A.; Sakamoto, J. Intergranular Li Metal Propagation through Polycrystalline $Li_{6.25}Al_{0.25}La_3Zr_2O_{12}$ Ceramic Electrolyte. *Electrochim. Acta* **2017**, *223*, 85–91.

(78) Sharafi, A.; Haslam, C. G.; Kerns, R. D.; Wolfenstine, J.; Sakamoto, J. Controlling and Correlating the Effect of Grain Size with the Mechanical and Electrochemical Properties of $Li_7La_3Zr_2O_{12}$ Solid-State Electrolyte. *J. Mater. Chem. A* **2017**, 21491–21504.

(79) Cheng, E. J.; Taylor, N. J.; Wolfenstine, J.; Sakamoto, J. Elastic Properties of Lithium Cobalt Oxide ($LiCoO_2$). *J. Asian Ceram. Soc.* **2017**, *5*, 113–117.

(80) Cheng, E. J.; Hong, K.; Taylor, N. J.; Choe, H.; Wolfenstine, J.; Sakamoto, J. Mechanical and Physical Properties of $LiNi_{0.33}Mn_{0.33}Co_{0.33}O_2$ (NMC). *J. Eur. Ceram. Soc.* **2017**, *37*, 3213–3217.

(81) Maxisch, T.; Ceder, G. Elastic Properties of Olivine Li_xFePO_4 from First Principles. *Phys. Rev. B - Condens. Matter Mater. Phys.* **2006**, *73*, 1–4.

(82) Qi, Y.; Hector, L. G.; James, C.; Kim, K. J. Lithium Concentration Dependent Elastic Properties of Battery Electrode Materials from First Principles Calculations. *J. Electrochem. Soc.* **2014**, *161*, F3010–F3018.

(83) Sakuda, A.; Hayashi, A.; Takigawa, Y.; Higashi, K.; Tatsumisago, M. Evaluation of Elastic Modulus of Li_2S–P_2S_5 Glassy Solid Electrolyte by Ultrasonic Sound Velocity Measurement and Compression Test. *J. Ceram. Soc. Japan* **2013**, *121*, 946–949.

(84) McGrogan, F. P.; Swamy, T.; Bishop, S. R.; Eggleton, E.; Porz, L.; Chen, X.; Chiang, Y.-M.; Van Vliet, K. J. Compliant Yet Brittle Mechanical Behavior of Li_2S-P_2S_5 Lithium-Ion-Conducting Solid Electrolyte. *Adv. Energy Mater.* **2017**, *7*, 1602011.

(85) Kato, A.; Yamamoto, M.; Sakuda, A.; Hayashi, A.; Tatsumisago, M. Mechanical Properties of Li_2S–P_2S_5 Glasses with Lithium Halides and Application in All-Solid-State Batteries. *ACS Appl. Energy Mater.* **2018**, *1*, 1002–1007.

(86) Yang, Y.; Wu, Q.; Cui, Y.; Chen, Y.; Shi, S.; Wang, R. Z.; Yan, H. Elastic Properties, Defect Thermodynamics, Electrochemical Window, Phase Stability, and Li^+ Mobility of Li_3PS_4: Insights from First-Principles Calculations. *ACS Appl. Mater. Interfaces* **2016**, *8*, 25229–25242.

(87) Weber, D. A.; Senyshyn, A.; Weldert, K. S.; Wenzel, S.; Zhang, W.; Kaiser, R.; Berendts, S.; Janek, J.; Zeier, W. G. Structural Insights and 3D Diffusion Pathways within the Lithium Superionic Conductor $Li_{10}GeP_2S_{12}$. *Chem. Mater.* **2016**, *28*, 5905–5915.

View Article Online
DOI: 10.1039/C8EE00907D

(88) Wang, Z. Q.; Wu, M. S.; Liu, G.; Lei, X. L.; Xu, B.; Ouyang, C. Y. Elastic Properties of New Solid State Electrolyte Material $Li_{10}GeP_2S_{12}$: A Study from First-Principles Calculations. *Int. J. Electrochem. Sci.* **2014**, *9*, 562–568.

(89) Deng, Z.; Wang, Z.; Chu, I.-H.; Luo, J.; Ong, S. P. Elastic Properties of Alkali Superionic Conductor Electrolytes from First Principles Calculations. *J. Electrochem. Soc.* **2016**, *163*, A67–A74.

(90) Wolfenstine, J.; Jo, H.; Cho, Y. H.; David, I. N.; Askeland, P.; Case, E. D.; Kim, H.; Choe, H.; Sakamoto, J. A Preliminary Investigation of Fracture Toughness of $Li_7La_3Zr_2O_{12}$ and Its Comparison to Other Solid Li-Ionconductors. *Mater. Lett.* **2013**, *96*, 117–120.

(91) Ni, J. E.; Case, E. D.; Sakamoto, J. S.; Rangasamy, E.; Wolfenstine, J. B. Room Temperature Elastic Moduli and Vickers Hardness of Hot-Pressed LLZO Cubic Garnet. *J. Mater. Sci.* **2012**, *47*, 7978–7985.

(92) Herbert, E. G.; Tenhaeff, W. E.; Dudney, N. J.; Pharr, G. M. Mechanical Characterization of LiPON Films Using Nanoindentation. *Thin Solid Films* **2011**, *520*, 413–418.

(93) Kaye, L. Tables of Physical and Chemical Constants. *Handb. Physicochem. Prop. Elem.* **1968**, 387–446.

(94) Kaye, G. W. C.; Laby, T. H. Physical and Chemical Constants and Some Mathematical Functions. **1911**.

(95) Sizova, N.; Kim, S.; Kobayashi, H.; Parrini, L. Internal Friction and Creep-Recovery in Indium. *Le J. Phys. IV* **1996**, *6*, 7–9.

(96) Yi, T.-F.; Xie, Y.; Zhu, Y.-R.; Shu, J.; Zhou, A.-N.; Qiao, H.-B. Stabilities and Electronic Properties of Lithium Titanium Oxide Anode Material for Lithium Ion Battery. *J. Power Sources* **2012**, *198*, 318–321.

(97) Qi, Y.; Guo, H.; Hector, L. G.; Timmons, A. Threefold Increase in the Young's Modulus of Graphite Negative Electrode during Lithium Intercalation. *J. Electrochem. Soc.* **2010**, *157*, A558.

(98) Shenoy, V. B.; Johari, P.; Qi, Y. Elastic Softening of Amorphous and Crystalline Li-Si Phases with Increasing Li Concentration: A First-Principles Study. *J. Power Sources* **2010**, *195*, 6825–6830.

(99) Pugh, S. F. XCII. Relations between the Elastic Moduli and the Plastic Properties of Polycrystalline Pure Metals. *London, Edinburgh, Dublin Philos. Mag. J. Sci.* **1954**, *45*, 823–843.

(100) Kraft, M. A.; Culver, S. P.; Calderon, M.; Böcher, F.; Krauskopf, T.; Senyshyn, A.; Dietrich, C.; Zevalkink, A.; Janek, J.; Zeier, W. G. Influence of Lattice Polarizability on the Ionic Conductivity in the Lithium Superionic Argyrodites Li_6PS_5X (X = Cl, Br, I). *J. Am. Chem. Soc.* **2017**, *139*, 10909–10918.

(101) Krauskopf, T.; Pompe, C.; Kraft, M. A.; Zeier, W. G. Influence of Lattice Dynamics on Na^+Transport in the Solid Electrolyte $Na_3PS_{4-x}Se_X$. *Chem. Mater.* **2017**, *29*, 8859–8869.

(102) Bachman, J. C.; Muy, S.; Grimaud, A.; Chang, H.-H.; Pour, N.; Lux, S. F.; Paschos, O.; Maglia, F.; Lupart, S.; Lamp, P.; et al. Inorganic Solid-State Electrolytes for Lithium Batteries: Mechanisms and Properties Governing Ion Conduction. *Chem. Rev.* **2016**, *116*, 140–162.

(103) Muy, S.; Bachman, J. C.; Giordano, L.; Chang, H.-H.; Abernathy, D. L.; Bansal, D.; Delaire, O.; Hori, S.; Kanno, R.; Maglia, F.; et al. Tuning Mobility and Stability of Lithium Ion Conductors Based on Lattice Dynamics. *Energy Environ. Sci.* **2018**, *11*, 850–859.

(104) Noble, B.; Harris, S. J.; Dinsdale, K. The Elastic Modulus of Aluminium-Lithium Alloys. *J. Mater. Sci.* **1982**, *17*, 461–468.

View Article Online
DOI: 10.1039/C8EE00907D

(105) Reuss, A. Berechnung Der Fließgrenze von Mischkristallen Auf Grund Der Plastizitätsbedingung Für Einkristalle. *ZAMM□Journal Appl. Math. Mech.* **1929**, *9*, 49–58.

(106) Rosciano, F.; Christensen, M.; Eyert, V.; Mavromaras, A.; Wimmer, E. REDUCED STRAIN CATHODE MATERIALS FOR SOLID STATE LITHIUM ION BATTERIES. WO/2014/191018, 2014.

(107) Strauss, F.; Bartsch, T.; de Biasi, L.; Kim, A.-Y.; Janek, J.; Hartmann, P.; Brezesinski, T. Impact of Cathode Material Particle Size on the Capacity of Bulk-Type All-Solid-State Batteries. *ACS Energy Lett.* **2018**, *3*, 992–996.

(108) Wang, J.; Huang, Q. A.; Yu, H. Size and Temperature Dependence of Young's Modulus of a Silicon Nano-Plate. *J. Phys. D. Appl. Phys.* **2008**, *41*, 165406–165411.

(109) Rosero-Navarro, N. C.; Kinoshita, T.; Miura, A.; Higuchi, M.; Tadanaga, K. Effect of the Binder Content on the Electrochemical Performance of Composite Cathode Using Li_6PS_5Cl Precursor Solution in an All-Solid-State Lithium Battery. *Ionics.* **2017**, *23*, 1619–1624.

(110) Oh, D. Y.; Kim, D. H.; Jung, S. H.; Han, J.-G.; Choi, N.-S.; Jung, Y. S. Single-Step Wet-Chemical Fabrication of Sheet-Type Electrodes from Solid-Electrolyte Precursors for All-Solid-State Lithium-Ion Batteries. *J. Mater. Chem. A* **2017**, *5*, 20771–20779.

(111) Koerver, R.; Walther, F.; Aygün, I.; Sann, J.; Dietrich, C.; Zeier, W. G.; Janek, J. Redox-Active Cathode Interphases in Solid-State Batteries. *J. Mater. Chem. A* **2017**, *5*, 22750–22760.

(112) de Biasi, L.; Lieser, G.; Rana, J.; Indris, S.; Dräger, C.; Glatthaar, S.; Moenig, R.; Ehrenberg, H.; Schumacher, G.; Binder, J. R.; et al. Unravelling the Mechanism of Lithium Insertion into and Extraction from Trirutile-Type $LiNiFeF_6$ Cathode Material for Li-Ion Batteries. *CrystEngComm* **2015**, *17*, 6163–6174.

(113) Zaghib, K.; Simoneau, M.; Armand, M.; Gauthier, M. Electrochemical Study of $Li_4Ti_5O_{12}$ as Negative Electrode for Li-Ion Polymer Rechargeable Batteries. *J. Power Sources* **1999**, *81–82*, 300–305.

(114) Jung, Y. S.; Oh, D. Y.; Nam, Y. J.; Park, K. H. Issues and Challenges for Bulk-Type All-Solid-State Rechargeable Lithium Batteries Using Sulfide Solid Electrolytes. *Isr. J. Chem.* **2015**, *55*, 472–485.

(115) Busche, M. R.; Weber, D. A.; Schneider, Y.; Dietrich, C.; Wenzel, S.; Leichtweiss, T.; Schröder, D.; Zhang, W.; Weigand, H.; Walter, D.; et al. In Situ Monitoring of Fast Li-Ion Conductor $Li_7P_3S_{11}$ Crystallization Inside a Hot-Press Setup. *Chem. Mater.* **2016**, *28*, 6152–6165.